UNIVERSITAT POLITÈCNICA DE CATALUNYA
BARCELONATECH
Escola d'Enginyeria de Telecomunicació
i Aeroespacial de Castelldefels

# TREBALL DE FI DE GRAU

**TFG TITLE: Micro gas turbine intake design for test rig airflow adaptation and air mass flow measurement**

**DEGREE: Grau en Enginyeria de Sistemes Aeroespacials**

**AUTHOR: Pablo Alejandro Álvarez Cebrián**

**ADVISOR: Fernando Pablo Mellibovsky Elstein**

**DATE: October 21, 2019**

**Título:** Diseño de una campana de admisión para una micro turbina de gas en un banco de pruebas, para adaptar y medir el flujo másico de aire
**Autor:** Pablo Alejandro Álvarez Cebrián

**Director:** Fernando Pablo Mellibovsky Elstein

**Fecha:** 21 de octubre de 2019

**Resumen**

El objetivo de este trabajo es el estudio y diseño de un conducto conocido como campana de entrada. El proyecto está presentado en varias fases: revisión de literatura, diseño con herramienta CAD, simulación en CFD, ubicación de sondas y equipos de medición y finalmente presupuesto de construcción, ensamblaje y puesta en marcha.
En la primera fase de revisión de literatura, se ha estudiado qué son los bancos de prueba de motores a reacción, así como cuáles son los objetivos de las campanas de entrada y por qué son necesarias en éstos.
En la fase de diseño, se han diseñado tres distintas campanas teniendo en cuenta que la forma elíptica es la mejor según investigaciones previas. Las tres campanas son de dimensiones distintas. Basicamente, la diferencia entre ellas es la longitud del semieje mayor. Las campanas de entrada se han diseñado teniendo en cuenta que son para una micro turbina de gas (EvoJet B170 Neo). En la fase de simulación CFD, se han simulado las tres campanas diseñadas para saber cuál es la que mejor adapta el flujo de aire y obtener los resultados del caudal másico en posiciones distintas de la campana de entrada, en función de la variación de la presión estática de la salida. Para ello, lo que primero se ha hecho ha sido imponer una condición de presión total de una atmósfera en lo que es la entrada y exterior de la campana de entrada (101325 Pa) y en la salida de la campana de entrada se ha impuesto la condición de contorno de una presión estática de 100075 Pa. El objetivo era crear una succión de aire debido al gradiente de presiones. Esto se ha aplicado en los tres conductos. Finalmente, se ha decidido por optar a usar en el EvoJet el conducto 1. Para estudiar este conducto, diferentes presiones estáticas se han ido simulando en ella: desde los 99500 Pa hasta 93175 Pa, y posteriormente desde los 90000 Pa hasta los 50000 Pa. Además, la variación del campo de presiones y de la velocidad se ha estudiado en función del radio (r) a diferentes localicaciones (x) a lo largo del conducto. Esto es, se ha estudiado v (r,x) y p (r,x). También se ha estudiado como varía la presión estática y total y la velocidad a lo largo del conducto (distintas secciones transversales), para ello se ha visto qué valor toman ciertos puntos localizados a lo largo del conducto.
La siguiente fase ha consistido en la colocación de sondas para obtener una buena estimación del caudal másico. El equipo necesario de sondas, así como la ubicación han sido justificados. También los instrumentos de medición.
La última fase del proyecto ha consistido en la creación de un presupuesto de construcción, ensamblaje y puesta en marcha. Para ello, se ha estudiado brevemente las propiedades físicas de diversos materiales para saber cuál merece la pena desde el punto de vista económico y cualitativo. El resultado ha sido el de aluminio 6061 y nylon. Por ello, se ha contactado con una fábrica para la elaboración de un presupuesto para la campana de entrada si el material de creación es aluminio 6061 y nylon. Para el presupuesto de las sondas y equipos de medición, se ha optado por buscar por la web qué equipos permiten operar en las condiciones simuladas con el software de CFD.

**Title :** Micro gas turbine intake design for test rig airflow adaptation and air mass flow measurement

**Author:** Pablo Alejandro Álvarez Cebrián

**Advisor:** Fernando Pablo Mellibovsky Elstein

**Date:** October 21, 2019

**Overview**

The objective of this work is the study and design of a bell mouth inlet duct. The project is divided in several phases: literature review, design with CAD tool, simulation with a CFD tool, location of probes and measuring equipment and finally construction, assembly and commissioning budget.

In the first phase of the literature review, it has been studied what are test rig facilities, as well as the objectives of bell mouth inlet ducts and why are necessary.

In the design phase, three different bell mouths have been designed taking into account that the elliptical streamwise radial cross-section for a bell mouth is the best according to previous studies. The three bell mouths have different dimensions (basically, the difference among them is the length of the semi-major axis). Moreover, the bell mouth inlet ducts have been designed taking into account that should be able to work with the micro gas turbine EvoJet B170 Neo.

In the CFD simulation phase, the three bell mouth inlet ducts have been simulated to know which one is better in terms of air flow adaptation and the results of the air mass flow at different locations when changing outlet static pressures. Firstly, the total pressure has been maintained constant at 1 atm (101325 Pa) and at the bell mouth outlet, a static pressure of 100075 Pa has been imposed so that the pressure gradient has created a suction of the air. Finally, it has been decided to choose to use bell mouth 1 in the EvoJet. Different static pressures from 99500 Pa to 93175 Pa, and then from 90000 Pa to 50000 Pa have been imposed to study the air flow behavior through out the bell mouth at different velocities. Moreover, the velocity and pressure variation in function of the radius at different locations x along the inlet have been studied: v(r,x) and p (r,x). It has also been studied how changed the velocity and pressure values along the duct at different gradient pressures studying the values of points located along the duct.

The next phase has been the placement of probes to obtain a good estimation of the air mass flow. The necessary probe equipment as well as the location have been justified. Also the measuring instruments.

The last phase of the project has been the construction, assembly and commissioning budget. To do it, the physical properties of various materials have been studied briefly to know which is the best material from an economic and qualitative point of view. The result has been 6061 aluminum and nylon. For this reason, a factory has been contacted in order to know which is the price for creating an aluminum 6061 bell mouth, and a nylon bell mouth. The probes prices have also been included in the total sum price of the budget.

# CONTENTS

# LIST OF FIGURES

# LIST OF TABLES

# LIST OF ABBREVIATIONS

## 0.1.. Nomenclature and symbols

$\mathbf{A_9}$ is the outlet area of the engine sketch.
**D** is the characteristic length of geometry.
$\mathbf{D_a}$ is the additive drag.
$\mathbf{dA_c}$ is a small area element.
$\mathbf{D_{fe}}$ is the external friction drag.
$\mathbf{D_{pe}}$ is the pressure drag.
**E** is the Young modulus.
**F** is the Thrust force.
**G** is the shear modulus.
**g** is the acceleration of gravity.
**K** is Kelvin.
**M** is Mach.
**Ma** is Mach.
$\dot{\mathbf{m}}$ is the air mass flow rate.
$\dot{\mathbf{m}}_\mathbf{0}$ is the inlet air mass flow rate of the engine sketch.
$\dot{\mathbf{m}}_\mathbf{9}$ is the outlet air mass flow rate of the engine sketch.
**p** is pressure.
$\mathbf{p_0}$ is the atmospheric pressure.
$\mathbf{p_1}$ is the pressure at a point 1 (bell mouth intake).
$\mathbf{p_2}$ is the pressure at a point 2 (bell mouth outlet).
**R** is the universal constant of ideal gases.
**Re** is the Reynolds number.
**T** is the air temperature.
**u** is the velocity value of the fluid.
**v** is the velocity of the sound at a medium.
$\dot{\mathbf{V}}$ is the volumetric air flow rate.
$\mathbf{V_{avg}}$ is the average velocity value of the fluid.
$\mathbf{V_0}$ is the inlet velocity at the engine sketch.
$\mathbf{V_1}$ is the velocity at a point 1 (bell mouth intake).
$\mathbf{V_2}$ is the velocity at a point 2 (bell mouth outlet).
$\mathbf{V_9}$ is the outlet velocity at the engine sketch.
$\mathbf{V_n}$ is the normal velocity of the fluid.
$\mathbf{Z_1}$ is the velocity at a point 1 (bell mouth intake).
$\mathbf{Z_2}$ is the height of a point 2 (bell mouth outlet).
$\alpha$ is the coefficient of linear thermal expansion.
$\gamma$ is the the adiabatic coefficient.
$\varepsilon$ is the turbulent dissipation rate.
$\kappa$ is the turbulent kinetic energy.
$\mu$ is the entrainment ratio; or the dynamic viscosity of the fluid.
$\rho$ is the air density.
$\sigma$ is the tensile strength.
$\upsilon$ is the Poisson ratio.

$\psi$ is the angular position of the probe.

## 0.2.. Acronyms and abbreviations

**CAD**: Computer-aided design.
**CFD**: Computational Fuid Dynamics.
**DES**: Detached Eddie Simulation.
**EETAC**: Castelldefels school of telecommunications and aerospace engineering.
**FVM**: Finite-Volume method.
**LES**: Large Eddie Simulation.
**Outl**: Outlet
**Press**: Pressure
**RANS**: Reynolds Average Navier-stokes.
**RBT**: Resistance bulb thermometer.
**RBT**: Resistance bulb thermometer.
**St.**: Static.

# ACKNOWLEDGEMENT

Firstly, I would like to express my special thanks of gratitude to my parents, who gave me the opportunity to study away from home. Also, because of their unconditional support.

Regarding the project, thank to Jose Castan and specially Francisco López, because they gave me advice and support with the CAD software. They helped me with the doubts I had when designing the solid and with the CFD tool.

And last but not least, to Fernando Mellibovsky, who advised and guided me during the project development.

# INTRODUCTION

With the arrival of gas turbine engines for aeronautical purposes, engine test facilities have become an important place for the assessment of a proper functioning of the engines.

To avoid problems measuring basic engine parameters such as thrust, or even damage of engine inlet blades, the use of bell mouths is very important.

Bell-mouth inlet ducts are a specially constructed channels used to direct air into the inlet of a gas turbine engine, for testing. Bell-mouth inlets are installed on engines being calibrated in a ground test stand, to guide air into the inlet guide vanes of the compressor.

This type of ducts allows the air flow to be funneled so that it enters without distortion in the engine, and when conditioned, the measurements are not affected by any distortion or vortex effects.

The inlet is a one-piece structure that conditions the air entering the engine's fan and enables accurate airflow measurement during on-ground rig testing.

## OBJECTIVE

The EETAC (UPC, Castelldefels) has acquired a micro gas turbine (EvoJet B170 Neo). The objective of this project is to design and study a bell mouth inlet duct which will be implemented on the EvoJet B170 Neo to make accurate measurements of air mass flow.

With the use of CAD tools, several bell mouths are being designed taking into account the best geometric shape according to previous researches. Then, the simulation with CFD tools take place. Taking into account the appropriate boundary conditions on a test facility, results are obtained to know which one adapts better the flow. In addition, the air mass flow as well as the pressure field p(r,x) and velocity v(r,x) are computed.

Subsequently, the location of probes is proposed to to measure the total and static pressure, to obtain a good estimation of the air mass flow.

Finally, an analysis of the physical properties of various materials for the construction of the bell mouth and an assembly budget is made (also taking into account the measuring equipment) for the total cost of the project.

It is important to remark that this project is going to be continued by students of UPC. In this case, the project stops at the preliminary design and preliminary budget.

# CHAPTER 1. AERONAUTICAL ENGINES' TEST FACILITIES

The main aim of engine test facilities is to assess the engine performance under certain conditions. There are two types:

- Sea-Level Test Facility

- Altitude Test Facility

The most common is a Sea-Level Test Facility. So the work is focused on this kind of Test Facility.

## 1.1.. Sea-Level Test Facilities

This type of Facility test is more common because its cost is much cheaper. Simulating the proper conditions is more feasible, too.

There are two types of Sea-Level Test Facilities for testing gas turbine engines:

-Outdoor Stands

-Indoor Stands or closed test cell

Regarding the first type, the outdoor Stands, the main advantage of these kind of stands is that they allow for tests that cannot be performed indoors, such as bird ingestion, water ingestion, noise production or side wind tests. However, the main problem is that are dependent on ambient conditions, so the data collection may be affected by humidity, rain, and wind; and also normally these kind of Stands are louder than the indoor test cells, for this reason these types of cells are located in remote areas with difficult access.

An outdoor cell consists in basically an open air Stands that supports the engine, providing measurements. The test bed area should be separated and free of any obstacle that could affect the test performance. To avoid inlet interferences, the engine is elevated and supported by a Stand. The effects of the cross wind are neglected using a large mesh screen fitted on the inlet. The EvoJet B170 Neo will be tested on outdoors.

Regarding the second type, the indoor cell, consists usually in a cell test where the engine is tested without external conditions such as wind or humidity. Obviously, the reading of measurements (air mass flow, Thrust...) will not be as accurate as it would be if it was performed outside, because of the flow field generated by walls for example (aerodynamic problems related to cells). Turbofan and Turbojets are normally assessed in this type of test facilities.

Other possible test flight conditions are performed in a flying test bed where the engine is mounted on an aircraft, look Figure 1.1. This has some advantages [1] like:

-Better simulations in terms of quality regarding inlet distortion.

-Low cost.

-High availability, independent of water conditions.

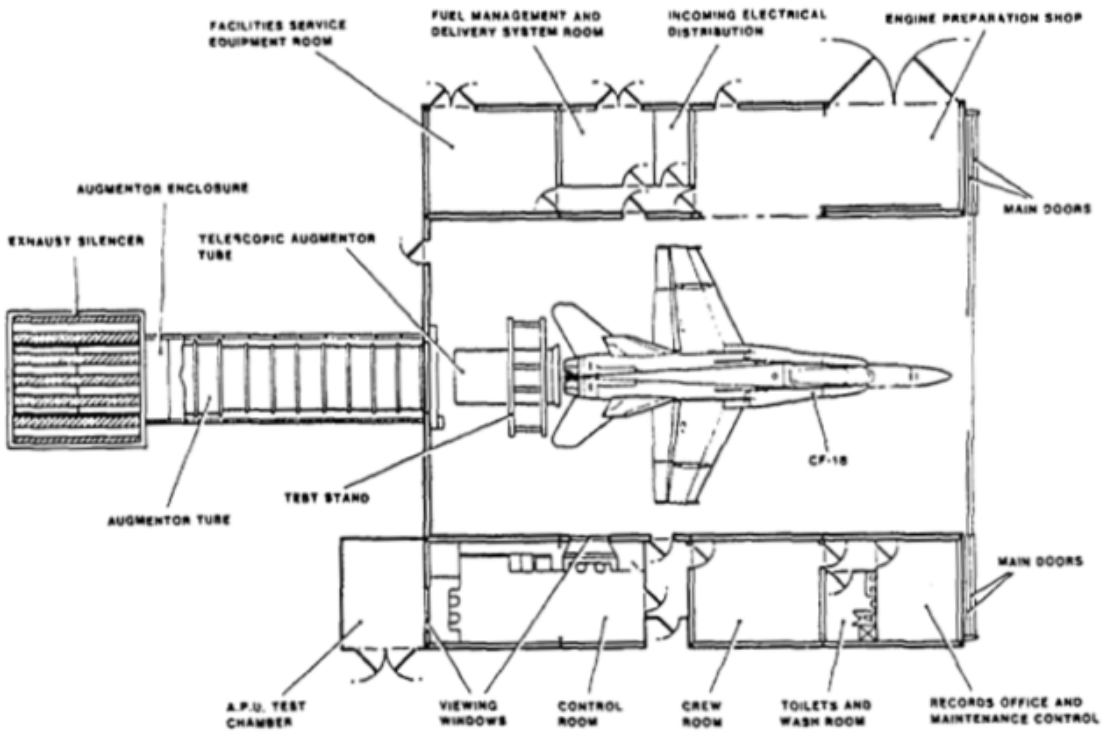


Figure 1.1: Top view of a flying test bed sketch, the engine to assess is mounted on an aircraft(Jaques 1984) [2]

There are some parameters that are very important to ensure in a a test bed as is said in [1]

-Engine inlet flow is uniform. Any distortion will affect the engine performance and give inaccurate air mass flow measurements. Also, avoid vortex generation from the floor or by the walls, causing serious problems at compressor blades.

-There is not re ingestion of exhaust gases. This could cause a distortion at inlet temperature, affecting the quality of the measurements.

-Static pressure field around an engine is as close to that of free stream conditions.

-The static pressure distribution at the propelling nozzle exit allows accurate determination of a mean value.

Figure 1.2 show an engine installation on a thrust bed. Figure 1.3 show open and enclosed test facilities.

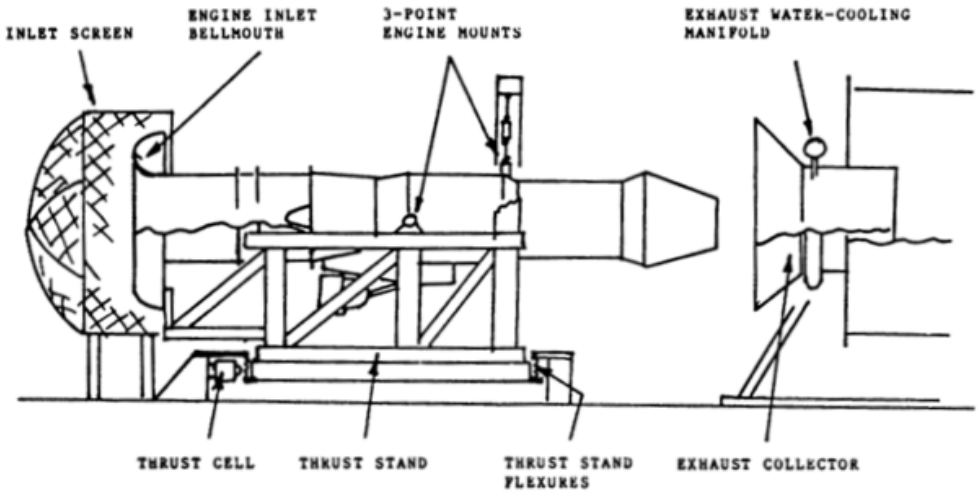


Figure 1.2: Engine installation on a thrust bed (Jaques 1984) [2]


(a) Open sea-level test facility

(b) enclosed sea-level test facility

Figure 1.3: Open and enclosed test facilities (Jaques 1984) [2]

## 1.2.. Bell mouth Inlet Ducts

During indoor and outdoor sea-level test, a bell mouth inlet duct is attached to the stand as intake. These convergent inlet-air ducts, provide a smooth curve for the induction air when flowing into the compressor and the duct losses are lower than it would be if the test was performed without it.

Basically, the main objective of bell mouths are related with engines' performance measurements. Without them, larger quantities of flow at the inlet is not conditioned, causing pressure losses between the outside of the bell mouth and the inside (static pressure), leading to incorrect measurements.

Bell mouths are very useful when the uninstalled thrust is being calculated. Also, regarding flow phenomena, it is important to smooth the inlet flow in order to prevent incorrect measurements due to flow separation and distortion; because the Thrust measurement are influenced by these parameters.

Bell mouths can also be supported with a large mesh screen fitted around the engine to protect the inlet of external elements that could be absorbed (screws, for instance).

Figure 1.4: Rig Test (bell mouth at engine inlet, courtesy of Rolls-Royce)

In figure 1.4, can be seen the bell mouth inlet duct with some pressure probes.

## 1.3.. Aerodynamic events on closed test facilities

There are some aerodynamics events can affect the engine during tests on closed test facilities, and it is important to know that the bell mouth inlet duct could prevent for instance vortex ingestion from the flow originated inside the cells. The importance of well-designing the indoor tests cells to prevent flow distortion, but also to attach a bell mouth inlet duct to the engine to avoid damage on blades and to get accurate measurements, is valuable.

### 1.3.1.. Flow Distortion

Flow distortion is basically is a problem related to the uniformity and smoothness of the flow. It is important to guarantee a uniform profile of flow to accurately assess pressure and temperature in order to obtain e.g. air mass flow rate. Flow distortion may generate vortex and asymmetric pressure distribution in the engine inlet.

The air velocity at the test cell affects the static pressure along the engine. The secondary flows (caused by the ejector action of the jet stream from the engine exhaust that enters the exhaust collectors) should not exceed 10 m/s because can produce change in the static pressure requited for measurements. [6]

The secondary flows have a big impact on engines' performance because it influences the most part of the flow phenomena which takes place inside the cell (not only flow distortion, but also vortex formation, recirculation, cell depression...) This is why entrainment ratio defined as $\mu$ , the ratio between primary and secondary flow, is a relevant parameter in terms of flow phenomena.

Pressure losses which the flow experiences passing through inlet plenum is also a parameter that has to be taken into account. Loss in total pressure along inlet system can be reflected in cell depression inside the cell and it could affect the flow uniformity around the engine, so it would affect the measurements' quality. The recommendation is that 150 mm of H20 (Pa) should be the limit. [2]

### 1.3.2.. Flow separation and vortex ingestion

The separation of the flow from the walls, has a negative impact in both engine performance and quality of the flow inside the cell, and can lead to vortex ingestion by the engine. In figure 1.5 can be seen a vortex ingestion during an on-ground test.

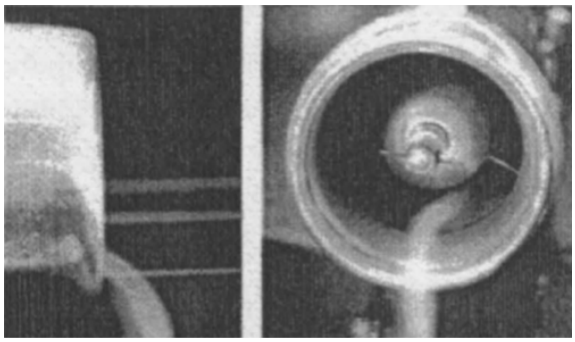

Figure 1.5: Vortex ingestion (fog visualization) during engine's tests,(Brix, Neuwerth, and Jacob 2000) [7]

## 1.4.. Pressure measurement devices

Older test beds have used water or mercury manometers, where the height of a column of liquid in a gas tube was read visually [1]. Smalls corrections were applied to the temperature of the liquid column. This way of pressure measurement has disappeared because nowadays automatic data recording is prevalent.

In modern test beds, transducers are used for pressure measurements. A transducer is based on pressure differences, which causes movement of a diaphragm and converts this into an electrical signal (voltage). The other side of a diaphragm is at ambient pressure (giving gauge reading pressure) or vacuum (giving absolute reading pressure). An electrical signal is related to pressure levels (either a dead weight tester applier a known force, this is, air pressure; or by comparison with other transducers). Temperature transducers should be controlled to avoid accuracy problems.

Typical accuracies are 0.1% at full scale (basic transducer); but a good overall accuracy demands 0.5% for engine pressures [1].

Regarding the ambient pressure, there exist two types of barometers to measure it: an Aneroid and mercury glass (Fortin Barometer). The latter is read visually, and the previous is read in a dial, which has a point controlled by an evacuated metal cylinder with corrugated sides. [1]

If the test is performed inside a test bed, test cell static pressure is required. It is measured in at least two places with low cell velocity. Usually, at the nozzle exit (side walls) at engine centerline height. Basically, test cell static pressure measurement consists on a 1-2mm diameter capillary tube surrounded by a pot called "pepper pot" and which removes the incident velocity effects. This tube is then connected to a transducer.

Regarding the total pressure, if the test is performed outdoors, it is the ambient pressure. If the test is performed indoors, it is the cell pressure. Total pressure rakes with wall static tappings normally are used in combination on the same plane. This combination is done because at the walls, static pressure is equal to the total pressure. If the static pressure is uniform, (low swirl angle) and uniform profile of the flow, the difference between static and total pressure indicates the flow velocity, necessary to obtain mass flow. [1]

Test cell ambient pressure is usually considered to be control room barometric pressure in the control room adjusted for cell depression. It may be used for inlet total pressure if the

air velocity in the cell is low, and an allowance is made for screen loss. High cell velocities, in excess of 8 meters per second, will require a calibration between inlet total pressure and a cell wall static pressure located upstream of the bell mouth.

There are other pressures that can be measured like Transient Pressures, Dynamic Pressures but which not will be explained because there have not a great effect regarding inlet mass flow measurement in comparison with the other pressures explained above.

Total and static pressures are read in a duct of known area, usually where contraction occurs and increases the dynamic head, along with total temperature. Measurements may also be taken at other stations, and where direct measurement is not possible calculations are performed based on flow continuity using design air system assumptions. [3]

## 1.5.. Temperature measurement devices

Temperature measurements provides an important information for air mass flow measurement. Also, temperature measurement is required in order to assess overall engine performance, define efficiency and flow capacity of a component, to ensure mechanical integrity (to know if the temperature limit of the engine is being exceeded) and so on and so forth.

It is well-known that temperature measurement is not an easy task, and it is often difficult to find how to measure static temperature because it is normally computed the total temperature (purely static pressure does not exist at all). [1]

It is worth to remind that total temperature is referred in terms of static and dynamic components (intern energy and kinetic energy). If a fraction of intern energy is converted into kinetic energy, static temperature would decrease.

Since engine performance is quite sensitive to inlet temperature, it is extremely important to accurately measure that temperature. An average inlet air temperature can be obtained by locating a sufficient number of sensors ahead of the engine inlet. To assess the temperature, usually resistance bulb thermometer (RBTs) are used (sometimes with thermocouples or snakes) and mounted on test cell splitters or in Debris Guard.

Cell design and cooling is also relevant, because exhaust gas may be re-ingested into the inlet and the results could become inaccurate.[2]

### 1.5.1.. Resistance Bulb Thermometers (RBT)

Inlet temperature is measured by changes in the resistance of a heated material which normally is platinum [1]. They are suitable for measuring temperatures up to 1000K and with high accuracy around 0.1 K. The main disadvantage is that are very delicate.

At least 3 Resistance Bulb Thermometers are recommended [2] to measure air inlet temperature during a test in a Test Bed if there are not suspects of non-uniform temperature profile.

### 1.5.2.. Snakes

Snakes are temperature devices, which consist in long resistance thermometers. Due to the big dimensions, an accurate calibration is not an easy task and this is the reason of why multiple RBTs are preferred instead. An indicative accuracy is between 1-2 K [1]

### 1.5.3.. Thermocouples

The main advantage of this device is that are more robust but with worser accuracy than RBTs.

There are different thermocouples, producing different voltage curves. There are also different classes of thermocouples based on the tolerances to voltage curves. For example, type 1 have 0.4% of tolerance, type 2, 0.75% [3]. The higher is the working temperature, the bigger is the inaccuracy. This explains why RBTs are preferred.

In figure 1.6 a sketch of a bell mouth inlet duct with thermocouples and pressure rakes is shown.

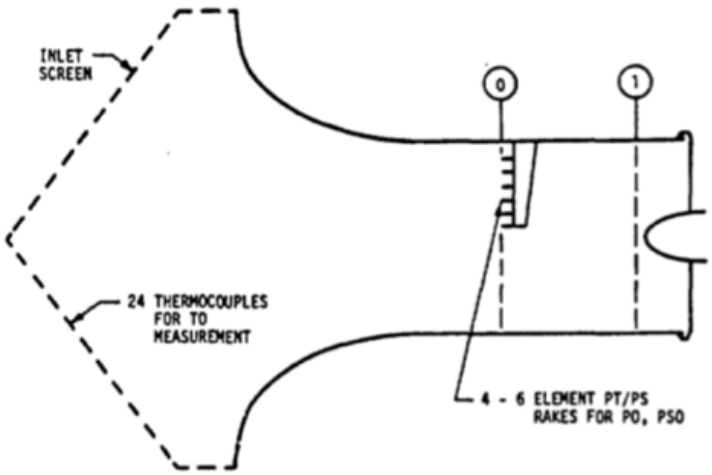


Figure 1.6: Longitudinal view of a bell mouth inlet duct, with thermocouples and pressure rakes.(Walsh, Fletcher) [3]

## 1.6.. Airflow measurement

The importance of measuring the air mass flow during a test rig eradicate in:

-The importance of determining momentum drag and also specific fuel consumption, for example.

-Temperature levels in the combustion can only be determined from air mass flow, and also from fuel energy flow or combustor inlet temperature.

-To determine the exhaust gas power, air mass flow is necessary during shaft power testing.

-To determine the compressor surge margins, air mass flow needs to be known. [2]

From bell mouth characteristics and measurements of pressure (inlet static pressure, inlet total pressure, ambient barometric pressure) and inlet temperature, airflow can be calculated.

Inlet total pressure has not the same value as barometric pressure, because there is a pressure drop across inlet screen [2]. By inlet total pressure and static pressure, differential pressure can be computed and thus air mass flow. The higher is the flow rate, the higher is the pressure differential [4]. Barometric pressure has also an important role, because it allow us to correct engine pressure data to standard day conditions.

By dividing the bell mouth section is smaller areas, the velocity profile could be obtained with higher accuracy. Each velocity area is computed by differences between static and total pressure, and this is done by putting pitot-static probes. Knowing the velocity distribution along each area, and the inlet temperature, we can obtain an accurate velocity profile and thus obtain the total air mass flow rate.

A reynolds number sensitive flow coefficient obtained by either calibrating against a reference meter or boundary layer measurements, modifies this value to yield an actual airflow. This is a rigorous and a high accuracy procedure that is necessary for a cell correlation program [3]. But in the case of a sea-level test indoor, inlet rakes are not installed because they need a great maintenance. An array of thermocouples attached to inlet screen are used to measure air temperature.

The measurement accuracy depends on the kind of device used. The most common devices for measuring air mass flow are during test rig are: venturi (most complicated but also the one giving the best accuracy); and the flare. [5]

On the one hand, the flare device is a short duct with a bell mouth, fitted at the front of the engine. With this device, a low-pressure drop is imposed to the engine. [3]

On the other hand, a venturi, it is a longer duct than the flare, and also has a diffusing section. The advantage of this device is that avoid some external effects generated by the engine.

The Venturi consists in a convering-diverging nozzle with an inlet section and a throat section, with a narrow cross sectional area [5]. Using the venturi, the total pressure must be measured through calibration. There are two type of venturi, the delta P, in which the difference between pressure at inlet and at the exit section is measured; and the critical venturi, which is used for choked flows (compressible) and therefore for a test rig for a light aircraft it is not used.

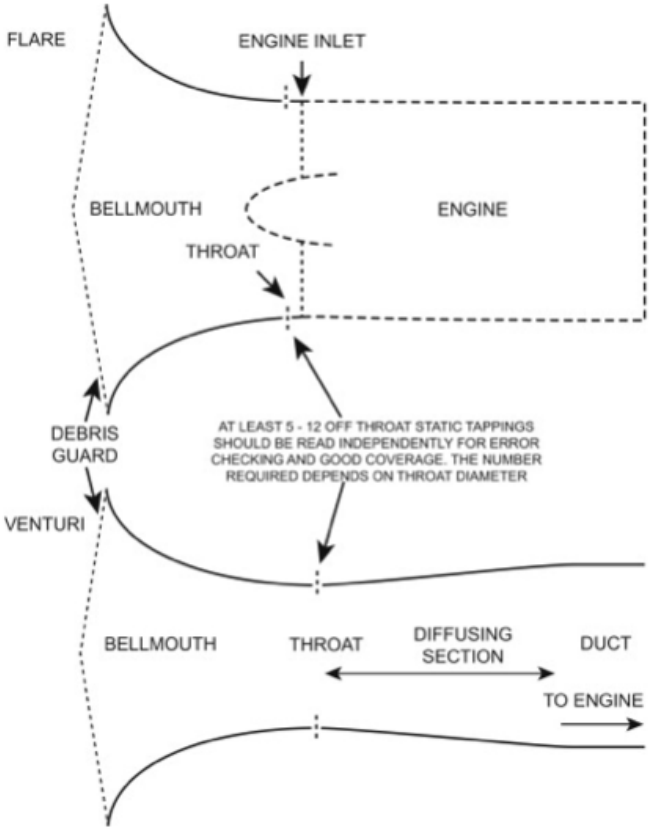


Figure 1.7: Venturi and flare devices (Walsh, Fletcher) [3]

In figure 1.7, venturi and flare devices are shown.

It is necessary to calibrate airflow instrumentation to obtain the accurate airflow that is flowing through the bell mouth inlet duct. Otherwise, the results obtained from the tests would not be valid.

## 1.7.. Thrust calculation

Thrust is the mechanical force that allows the movement of the aircraft through the air. This mechanical force, is generated by the aircraft engines.

This force is generated by the reaction of accelerated mass flow.

It is important to remark that during rig tests, the Uninstalled Thrust is the type of Thrust that is calculated. The difference between the Unistalled Thrust and the Installed Thrust, is that the real effects of Additive drag ($D_a$), External friction Drag ($D_{F_e}$) and External pressure drag ($D_{P_e}$) that affect the Installed Thrust, are negligible in the uninstalled Thrust.

$D_a$ , $D_{F_e}$ and $D_{P_e}$ only depend on:

- Flight conditions

- Nacelle geometry

- Aircraft/engine integration

Regarding the first type of drag, the Additive (inlet, ram) Drag:

$$D_a = \int_0^1 (p - p_0) dA \tag{1.1}$$

-where $p$ is pressure

-$p_0$ is the pressure upstream the control volume (station 0).

-dA is a differential portion of Area.

As already mentioned, it can be neglicted on ground during a test rig with an adapted intake (bell mouth inlet duct).

Regarding External pressure drag:

$$D_{p_e} = \int_1^9 (p_n - p_0) dA \tag{1.2}$$

is small in subsonic (no wave drag).

-where $p_n$ is the pressure of nacelle.

And finally, the External friction drag effect:

$$Df_e = \int_1^9 \tau_w P dx \tag{1.3}$$

which is negligible on ground.

-$\tau_w$ is the skin shear stress on a surface.

The equation of net installed thrust force:

$$F = \dot{m}_9 \cdot V_9 - \dot{m}_0 \cdot V_0 + (p_9 - p_0) \cdot A_9 - (D_a + D_e + D_{p_e}) \tag{1.4}$$

and if uninstalled, engine thrust equation 1.4 yields to:

$$F = \dot{m}_9 \cdot V_9 - \dot{m}_0 \cdot V_0 + (p_9 - p_0) \cdot A_9 \tag{1.5}$$

Also, if taking into account adapted nozzle ($p_9$ = $p_0$) the uninstalled thrust now is:

$$F = \dot{m}_9 \cdot V_9 - \dot{m}_0 \cdot V_0 \tag{1.6}$$

An illustrative engine sketch in figure 1.8

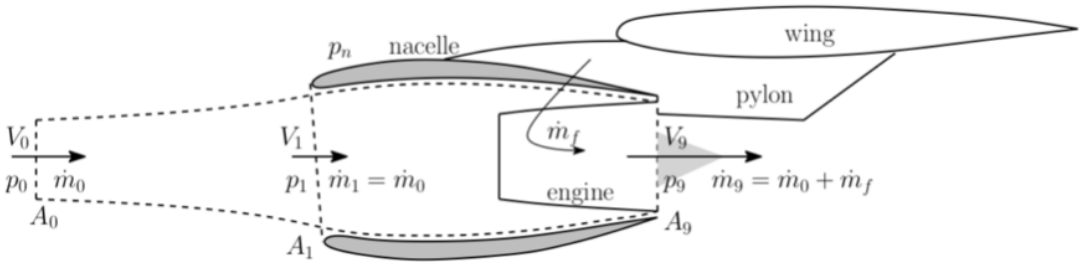


Figure 1.8: Basic engine sketch

# CHAPTER 2. SET UP OF CFD COMPUTATIONS FOR THE BELL MOUTH INLET GEOMETRY

The Computational Fluid Dynamics (CFD) is a branch of fluid mechanics that uses analysis and data structures to analyze and solve problems involving fluid flows systems, heat transfer, chemical reactions and other physical phenomena. The CFD solves the fluid flow equations in the domain of interest, specifying conditions.

The main objective of the CFD programs is to solve Navier-Stokes equations that describe the fluid behavior. As the analytic resolution of this equations is not possible (just some specific cases), CFD programs allow us to achieve it. For doing it, discretizing a region of space (spatial mesh) is required. Then, the discretized conservation equations are solved by the program.

When working with a CFD program, the following steps are always the same:

- CAD designing.
- Adequate Control volume designing.
- Quality meshing.
- Settings adjustment (boundary conditions, type of fluid, turbulent model, viscosity. . . ).
- Solving.
- Solution analysis. Basically check if the solution achieved has sense. If not, a revision and changes in some of the previous steps are required.

There are many advantages that these kind of programs provides, because we can solve the behavior of the fluid at different conditions and work regimes. In fact, being able to simulate a geometry with CFD programs is a good option in terms of economic and time savings. Before having a definitive model we can do several changes to achieve the adequate performances.

For simulating the fluid behavior on the several bell mouth designs, the CFD module on SOLIDWORKS was the option chosen. The main advantage of this module is that is integrated on SOLIDWORKS software. It is called Solidworks Flow simulation, and uses the Finite-Volume Method (FVM) to calculate the performances and capabilities of the body at simulation. [8]

Now, an advanced explanation of the steps in the following sections.

## 2.1.. Computer specifications

For all the software work the computer used has been the same. More concretely on EETAC, at class 231G. The edition is windows 10 Enterprise 2016 LTSB. The processor is an Intel (R) Core (TM) i7-6700 CPU @3.400 GHz. The Ram installed has 16.0 GB. The system type has a 64-bit operating system.

## 2.2.. CAD Designing

The first step to perform a CFD simulation is the creation of a CAD geometry. As the objective is to study the behavior and capabilities of different bell mouth inlet ducts, three different bell mouth inlet duct were designed.

There are some studies [9] that demonstrates that the best choice is the elliptical streamwise radial cross-section for a bell mouth inlet duct due the flow adaptability capability. In fact, bell mouths used in test rig facilities for assessing the engine performances, have an elliptical streamwise variation of the cross-sectional radius. Based on this, three bell mouth inlet ducts were designed in order to assess the air mass flow at the engine intake.

“Solidworks” has been used as CAD software in order to achieve this. This program allows engineers to design solids and study the behavior through its modules, make torsion as well as fluid or heat transfer simulations. The geometry and the simulations were performed in 3D because in this case a pure 2D problem is not so representative. 2D axysimmetric simulations could have been an option too, because the effects of a sideslip or angle of attack or the swirl induced itself by the compressor are not taken into account.

All the models designed had the same outlet diameter (50 mm) because of the dimensions of the micro gas jet turbine EvoJet B170 Neo (the dimensions have been measured with a caliper).

### 2.2.1.. Models designed

The first bell mouth designed had a semi-major axis of 49.77 mm; a semi-minor axis of 33.33 mm and the distance between the outlet of the bell mouth and the center of the ellipse was 30 mm. The inlet diameter was 66 mm. The length of the bell mouth was 79.77 mm.

The second model had also an elliptical profile, but the main difference is the dimension of the ellipse. In this case, a bigger semi-major axis was designed to see the effect on the flow.

The semi-major axis of the ellipse was 134.91 mm, and the semi-minor axis 50 mm. Again, the outlet of the bell mouth is 50 mm (In flat geometry 25 mm, but once the revolution is created around the horizontal axis, the result is 50 mm). The distance between the outlet of the bell mouth and the center of the ellipse was 30 mm. The inlet diameter was 150 mm. As the semi-major axis is bigger, the inlet diameter is bigger too. The length of the bell mouth was 164.91 mm.

The last model (the third one) is similar to the second one, but the main difference is that the semi-major axis is even bigger. The semi-major axis was 200 mm; the semi-minor axis was 50 mm. The inlet diameter was 150 mm too. The outlet diameter was also 50 mm as before and the distance between the outlet and the center of the ellipse was 30 mm as the previous bell mouths designs. The length was 250 mm.

Once created, the next step was to empty it. All three bell mouth inlet ducts had 2 mm of thickness.

The side views of the three bell mouth inlet ducts are shown in figure 2.1

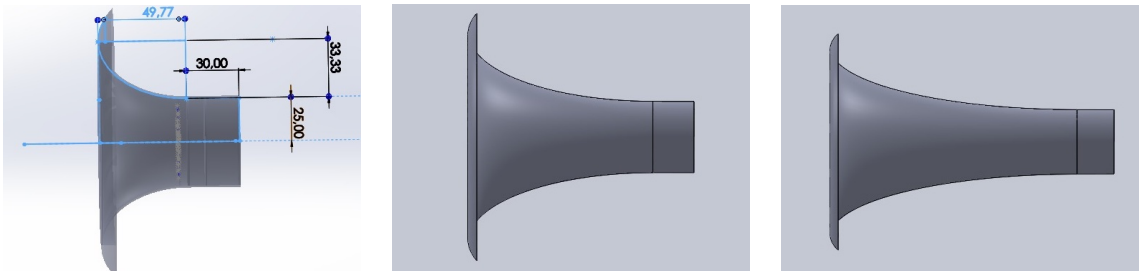


(a) Side view of the first bell mouth

(b) Side view of the second bell mouth

(c) Side view of the third bell mouth

Figure 2.1: Side views of the three bell mouth inlet ducts

The front views of the three bell mouth inlet ducts are shown in figure 2.2.

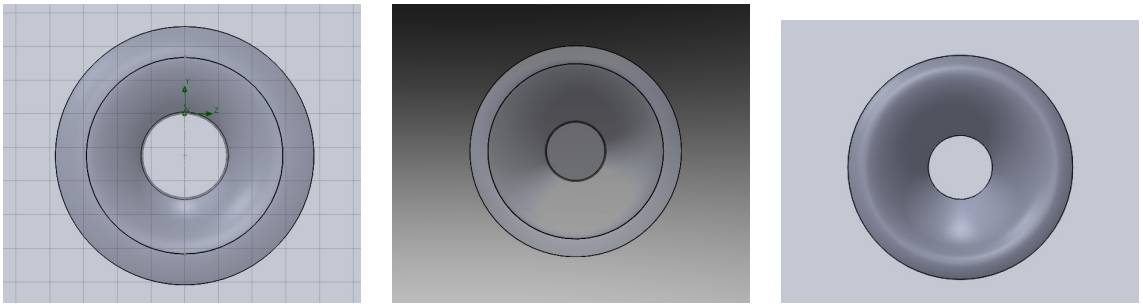

(a) Front view of the first bell mouth

(b) Front view of the second bell mouth

(c) Front view of the third bell mouth

Figure 2.2: Front views of the three bell mouth inlet ducts

A summary of the parameters of the three bell mouths is shown on the table 2.1

| Bell mouth | Parameters | Values |
|---|---|---|
| Bell mouth 1 | Semi-major axis | 49.77 mm |
| | Semi-minor axis | 33.33 mm |
| | Length | 79.77 mm |
| | Inlet Diameter | 66 mm |
| | Thickness | 2 mm |
| Bell mouth 2 | Semi-major axis | 134.91 mm |
| | Semi-minor axis | 50 mm |
| | Length | 164.91 mm |
| | Inlet Diameter | 150 mm |
| | Thickness | 2 mm |
| Bell mouth 3 | Semi-major axis | 200 mm |
| | Semi-minor axis | 50 mm |
| | Length | 250 mm |
| | Inlet Diameter | 150 mm |
| | Thickness | 2 mm |

Table 2.1: Summary of the values of main parameters at the three bell mouths

## 2.3.. Adequate Control Volume designing

In the Finite-Volume Method the conservation principles are applied to a fixed region in space known as a control volume. An adequate Control Volume is required to simulate the flow domain because the accuracy of results are influenced on it.

The control volume has also been created in Solidworks. The idea was to create a volume in which the air flux could be absorbed by the bell mouth from different directions. To achieve it, the control volume was designed as a semi-sphere. In other words, the bell mouth is inside a control volume that is a sphere cut by a plane.

Moreover, the control volume dimensions are the same for the different bell mouth models. The distance between the bell mouth intake and the inlet control volume would be kept constant along the different simulations. This is to ensure that the results are not influenced by the control volume and that in fact are simply due to the respective bell mouths.

This process was repeated for the three bell mouths, as can bee sen in figure 2.3

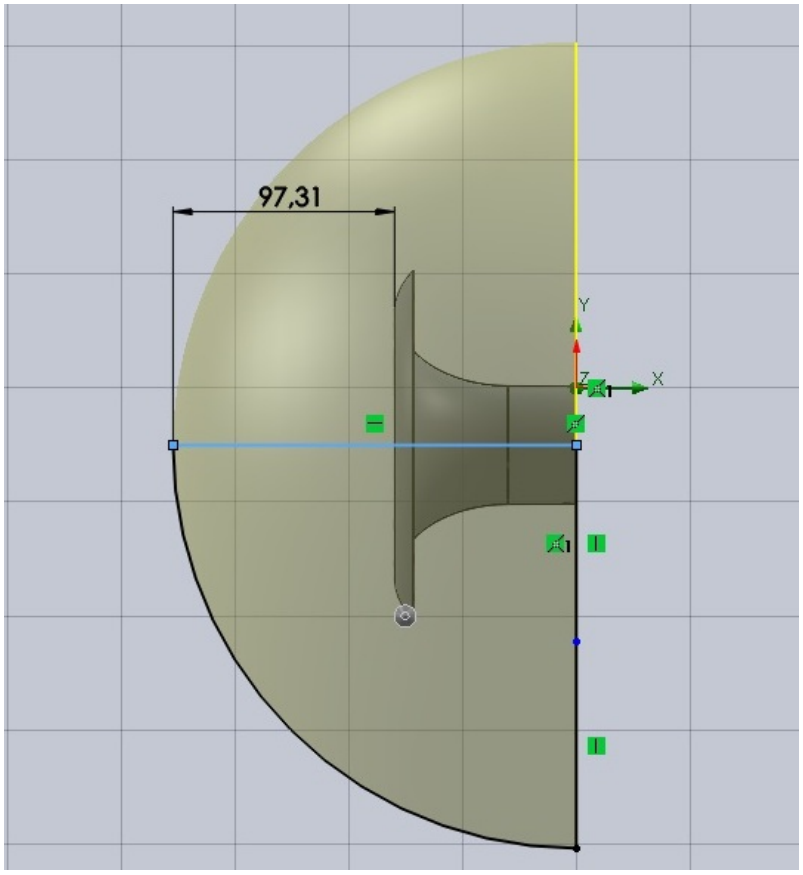


Figure 2.3: Control Volume, with the first bell mouth inside

## 2.4.. Initial settings of the problem

In this section, the initial settings are explained.

The initial settings is one of the most important steps because are the basis of the problem to be solved.

Once we have the solid designed and the Control Volume created, is time to start with the simulation section.

The International System of Units (SI) was the system of units selected to obtain the results. Three decimals for obtaining the velocity results and two decimals for the pressure results.

Regarding the type of analysis, between the two options of ”flows around bodies” (flows around a cylinder of around the wing of an air plane) and flows inside ducts (inside pipe ducts or as in this case, bell mouth inlet ducts) the option chosen was the latter. Because if we select the first case, the bell mouth would have been studied externally, not considering the flow crossing the duct inside. This is, the semi-sphere containing the bell mouth would have been considered as part of the solid to be studied, not as a control volume. Also, the exclusion of cavities without flow conditions was selected because we are studying the presence of the flow on the body.

Other physical aspects that we can choose are: heat conduction in solids, radiation, time independence, gravity, rotation or free surface. As what is being simulated is the behavior

of the fluid inside a bell mouth (which is in static conditions) none of the previous options were chosen.

Then we must select the type fluid to be simulated. There is a wide option of fluids that we can choose, for instance: gases (air, carbon dioxide, butane, hydrogen, ethanol...), liquids (the same mentioned and more), Non-Newtonian liquids (apple sauce, blood, olive oil...), compressible liquids, real gases and steam. As expected, the option chosen was air (in gas state).

Flow type selected was laminar and turbulent.

Regarding the turbulent flow, the flow characteristics on a turbulent flow simulation is solved with RANS (Reynolds Average Navier-Stokes). This turbulence model has less computational cost in comparison with others like DES (Detached Eddie Simulation) or LES (Large Eddie Simulation). There are several RANS models like K-epsilon, k-omega, SST, SAS, SST... The option chosen was k-epsilon for the simulation in CFD because of its minor requirements and good results. The turbulent parameters are: k which is the turbulent kinetic energy (measures the energy of the turbulent flow) and the epsilon $\varepsilon$, that determines the rate dissipation of the turbulent kinetic energy k.

For the simulations, as initialisation conditions, values of 1 J/kg for turbulent energy k and 1 W/kg for turbulent dissipation rate $\varepsilon$ were chosen (predetermined option).

A high mach number was not selected because hyper sonic conditions are not considered for testing the bell mouth inlet duct. The humidity was also not taken into account.

Finally, a “Global Coordinate System” was selected, with “x” as reference axis.

## 2.5.. Quality meshing

The meshing is one of the key stages of a CFD simulation. The main objective is to discretize the geometry. It is important to remark that there is a trade-off between the quality of the results and time for obtaining them (a good quality in results involve high computational effort while a poor quality results involve less computational effort).

Choosing the type of cells as well as the quantity is the most important part in this section.

It is important to mention that we can choose the geometry of the cell, for instance hexahedral, tetrahedral... There is a geometry that fits better depending on the shape of the geometry, or in the quality of the result that we want to obtain: while tetrahedral meshes can fit better complex geometry, hexahedral meshes are more economic in terms of computational efforts (six degrees of freedom for one hexahedral corresponds to six tetrahedral). But in my case, rectangular mesh was the option chosen with the cfd source tool (there is not option to choose hexahedral since it is Finite-element method).

Moreover, we can choose to create local meshes for specific regions. If we want to improve the resolution of certain zones because there is a specific region where the fluid property change, we can create finer meshes (an increase in the number of elements) and in zones with less relevance we can create coarser meshes (less number of elements).

It is important to mention that the Flow Simulation in Solidworks has the option of “Adaptative Meshing”. This allows the software to automatically refine certain area of high gradient, allowing to converge the results faster. But it is important to learn how to do it manually to choose the conditions that suits better in one geometry or in another.

Mesh generation begins by dividing the rectangular computational domain into a set of rectangular cells (cuboids) formed by the intersection of planes parallel to the axes of the coordinate system. A refinement implies to divide each cuboid in eight geometrically similar cuboids following several adaptation criteria which can be defined for each solid (curvature, narrow channels, small geometric elements, etc.) and automatically according to the solution gradients.

In the case of the bell mouth, as the shape is ”cylindrical”, the curvature option was chosen for the refinement. And as there are not little elements as skrews, it was not chosen the option of small geometric elements (the mesh was quite basic).

Regarding mesh quality: the mesh is divided in two sections: global and local meshing.

Global meshing takes into account the Control Volume and the solid that has to be simulated. There are nine levels of refined mesh: from 0 to 9. The more the level chosen, the better accuracy has the results but also the higher is the computational effort to achieve them. The global meshing chosen for our problem involved the semi-sphere.

The total number of cells was 118385.

The total number of cells is just the product between the number of cells in the respective directions. As the number of cells were too low to obtain a good convergence, the level of refinement needed to be increased.The channels’ refinement were imposed at a level of 5, and the advanced refinement also to 5. However, the main problem was that it was needed so much time for solving. Look at figure 2.4, in which for doing a first try with a pure 2D simulation (not correct for solving the bell mouth) it took more than 1 hour for 783 iterations. The same happened in 3D, it took more than an hour with a level 5 of

refinement (however just about 20 minutes to solve the problem in 3D). As there was not a great difference between the results at level 5 and level 4, and a great quantity of time was saved by changing to a lower level, the next election was a level 4 in both global and local meshes.

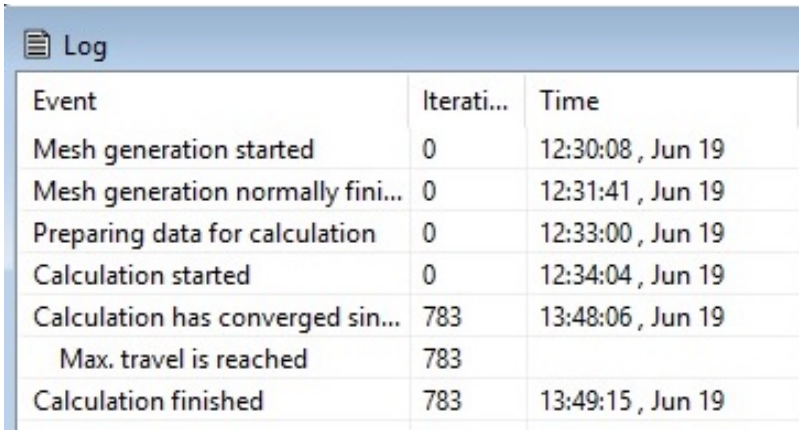
Log

| Event | Iterati... | Time |
|---|---|---|
| Mesh generation started | 0 | 12:30:08 , Jun 19 |
| Mesh generation normally fini... | 0 | 12:31:41 , Jun 19 |
| Preparing data for calculation | 0 | 12:33:00 , Jun 19 |
| Calculation started | 0 | 12:34:04 , Jun 19 |
| Calculation has converged sin... | 783 | 13:48:06 , Jun 19 |
| Max. travel is reached | 783 | |
| Calculation finished | 783 | 13:49:15 , Jun 19 |

Figure 2.4: 4 minutes for meshing and 783 iterations to converge, in 1h and 20 minutes (pure 2D)

For a level of 4 for refining the mesh, 400 iterations were needed to achieve convergence. In just 20 minutes the results are obtained. Look figure 2.5

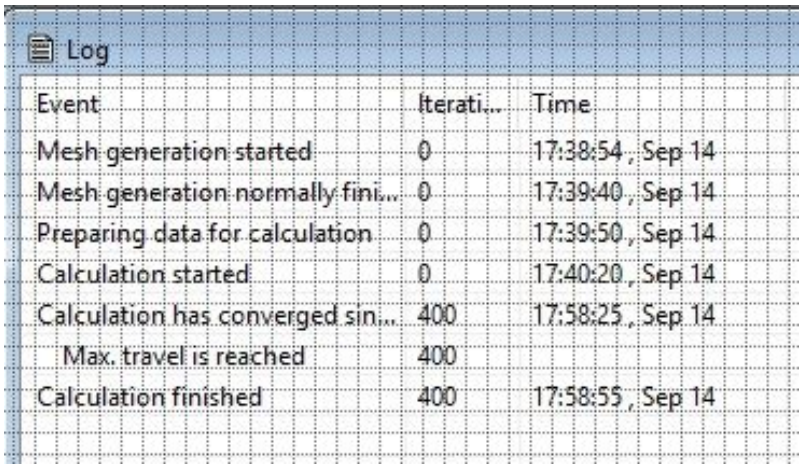
Log

| Event | Iterati... | Time |
|---|---|---|
| Mesh generation started | 0 | 17:38:54 , Sep 14 |
| Mesh generation normally fini... | 0 | 17:39:40 , Sep 14 |
| Preparing data for calculation | 0 | 17:39:50 , Sep 14 |
| Calculation started | 0 | 17:40:20 , Sep 14 |
| Calculation has converged sin... | 400 | 17:58:25 , Sep 14 |
| Max. travel is reached | 400 | |
| Calculation finished | 400 | 17:58:55 , Sep 14 |

Figure 2.5: 1 minute and 30 seconds for meshing and 400 iterations to converge, in just 20 minutes (3D)

Respect to local mesh, it serves for generating an specific mesh in certain zones to observe and assess better the fluid behavior there. Two local meshes were created to assess the outlet and the body of the bell mouth.A level 4 of local refinement was considered a good level because it was a good trade-off between accuracy and time for the bell mouth's body and for the outlet face. The level 4 of refinement was done with the option "curvature"

### 2.5.1.. Mesh assessing

As already commented, firstly a high number level of refinement was done in order to see if it was assumable. However, the large quantity of time to wait for the results and the little gain in accuracy was not worth at all. So if with a level 5 the computer needed 1 hour and a half, and with a level 4 just 20 minutes. Regarding the accuracy of the results, we have to compare the values obtained at the different levels of mesh refinement. Comparing the values obtained at an outlet static pressure of 100075 Pa:

The air mass flow rate at cross-section 1 with a level 5 of refinement was 0.0969 Kg/s and with a level 4 of refinement was 0.0971 kg/s At cross-section 2, the value of air mass flow rate with a level 5 of refinement was 0.0961 Kg/s and with a level 4 of refinement was 0.0969 kg/s. And at cross-section 3 with a level 5 of refinement a the value of air mass flow was 0.0963 Kg/s and with a level 4 the value was 0.0977 kg/s. In results section 2.7., the meaning of cross-sections are explained.

And, for example, the differences of velocity at the cross-section 1 with a level 5 of refinement, respect the level 4, is just 0.01 m/s (the difference is not really appreciable). Respect total pressure, the differences are a little bit higher, 2 Pa, but the quantity of time to obtain the result was not worth at all). Regarding the static pressure, the differences are of the order of magnitude of $10^{-1}$.

In figure 2.6 can be seen the result of the global mesh (control volume). The bell mouth inlet duct is inside.

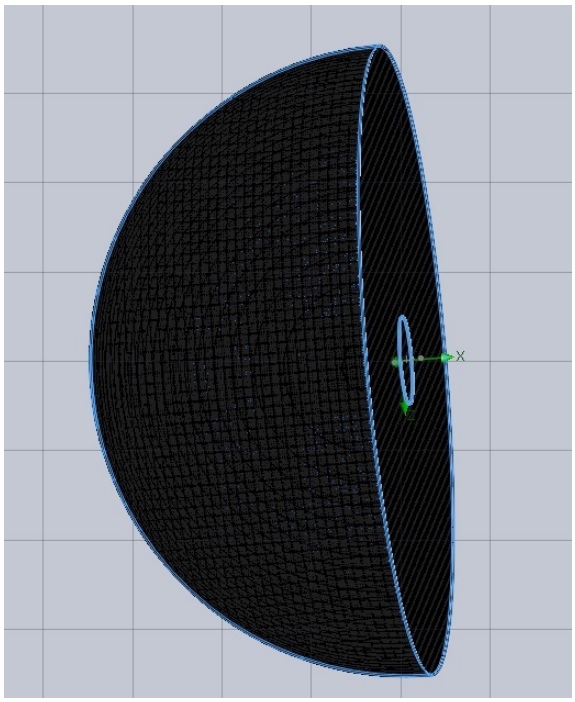


Figure 2.6: Mesh of the Control Volume (level 4 of refinement)

## 2.6.. Conditions' setup

In this section, the boundary conditions applied to the problem we wanted to solve and the physics of the fluid will be explained.

The computational Domain allow us to choose if we want to perform the simulation in 3D or in pure 2D or Axysimmetric 2D. As explained before, the bell mouth inlet duct problem is a 3D case and is more representative than the pure 2D simulations. The axysimmetric 2D simulations would have been correct too.

Regarding boundary conditions, note that is very important to establish realistic conditions to obtain meaningful data, this is, that the conditions of the problem could be those affecting the solid to simulate in reality. As we want to assess the fluid behavior on a bell mouth, it is important to define correctly the conditions for the bell mouth and for the Control Volume. So, the boundary conditions of the physical problem are these:

Control Volume: assuming that our bell mouth will work on an enclosed test facility, the conditions for the inlet and outlet region were: Total Pressure: 101325 Pa which is 1 atm (equivalent to the pressure exerted by the atmosphere at sea level). Regarding the Temperature, it was established 288,15K (equivalent to the temperature of a test facility, at 15 Celsius degrees). Note that no velocity was imposed ($V_0$ = 0) because the objective was to assess the velocity generated by pressure gradients. Moreover, these boundary conditions affect the inlet region and the outlet region of the Control Volume, but are not affecting the outlet of the bell mouth.

bell mouth walls: No-slip condition was imposed to the walls. In solidworks, it is called "real wall" condition. This was imposed because we know that real fluids "stick" to walls. The No-slip condition allows to simulate the fluid boundary layer on the bell mouth because the velocity starts out zero at the walls and as the thick of the boundary layer increases, the velocity increases. Just at the edge of the boundary layer, the velocity matches the incoming velocity (free velocity).

bell mouth outlet area: the condition imposed here was a static pressure 100075 Pa. The main scope is to assess the velocity at the outlet of the bell mouth ($V_2$) in order to obtain the air mass flow.

## 2.7.. Results discussion

In this section, the results of the different simulations that have been done, are commented.

Results of pressure and velocity contours as well as streamlines for the bell mouth 1 at an outlet static pressure of 100075 Pa can be found in annex A.

The results of maximum values of parameters like velocity and density on the three bell mouths at an outlet static pressure of 100075 Pa can be found here, in table 2.2

| bell mouth | Parameters | Values |
|---|---|---|
| bell mouth 1 | Max. Velocity | 44.932 m/s |
| | Min. Velocity | 0 m/s |
| | Max. Density | 1.2248 Kg/$m^3$ |
| | Min. Density | 1.2115 Kg/$m^3$ |
| bell mouth 2 | Max. Velocity | 45.147 m/s |
| | Min. Velocity | 0 m/s |
| | Max. Density | 1.2248 Kg/$m^3$ |
| | Min. Density | 1.2118 Kg/$m^3$ |
| bell mouth 3 | Max. Velocity | 44.94 m/s |
| | Min. Velocity | 0 m/s |
| | Max. Density | 1.2248 Kg/$m^3$ |
| | Min. Density | 1.2119 Kg/$m^3$ |

Table 2.2: Summary of maximum values of main parameters at the three bell mouths (at an outlet static pressure of 100075 Pa

These values correspond to maximum values achieved by bell mouth (not necessary in the outlet, just in some point through the duct).

As we can see, at the same conditions, the bell mouth 1 which was the first bell mouth designed had a maximum velocity of 44.932 m/s. The difference of maximum velocity achieved respect to the second bell mouth is 0.125 m/s and with the third one is almost the same (0.008 m/s of difference).

The maximum value of density achieved is the same for all three bell mouths (1.2248 kg/$m^3$).

The minimum velocity is 0 m/s for the three bell mouths since the inlet velocity boundary condition imposed to all three bell mouths was 0 m/s.

Bell mouth 1 was chosen as the bell mouth for the EvoJet B170 Neo since the streamlines showed that the flow was adapted correctly (Figure A.3) and there is not a high difference among the other ducts.

To know which is the best place to locate the static and total pressure probes in order to obtain a good estimation of the air mass flow, is convenient to study the pressure and velocity profiles in different points of the bell mouth.

To study pressure and velocity distribution along each cross-section (planes 1, 2, and 3) 8 radial lines were created at $\psi$ angles: 0º, 45º, 90º, 135º, 180º, 225º, 270º, 315º. See figure 2.8.
Cross-sectional planes 1 to 3, are located as shown in figure 2.7. The position of each

cross-sectional plane on the bell mouth, is shown in table 2.3.

Moreover, 40 points at different positions as shown in figure 2.7 were created along the three cross-sections, to study how the values of pressure and velocity changed along the duct and from walls to center. The value of total pressure, static pressure and velocity at each point (A to O') contained on each cross-sectional plane, at an outlet static pressure 100075 Pa; and curves (union of points crossing each plane) associated with each point (in order to see the profiles behaviors) is shown on tables C.1, C.3, C.4, and C.5 at the appendix C.

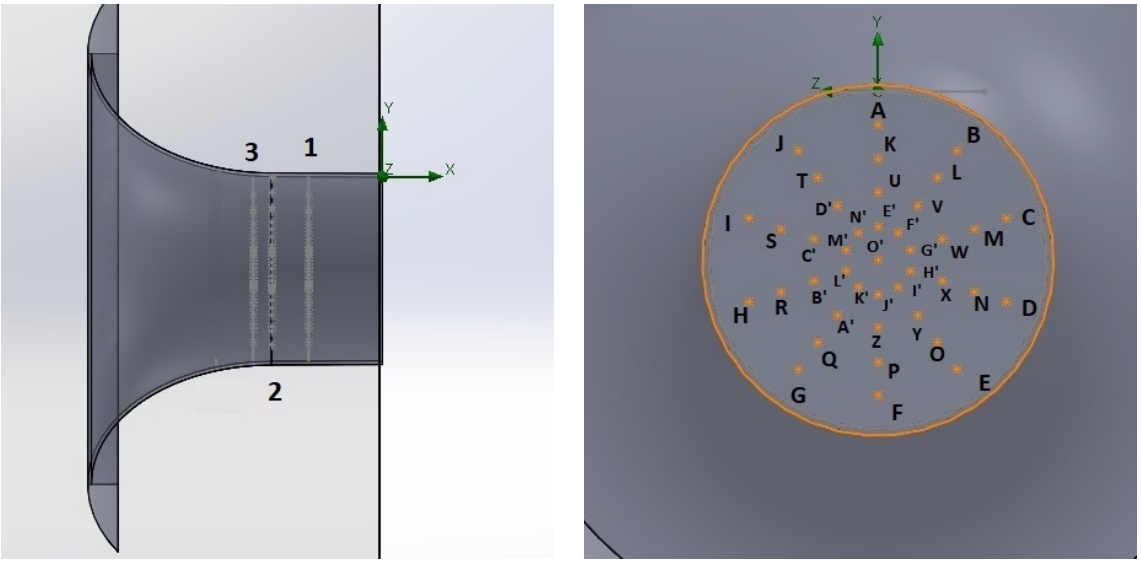


(a) The location of the three cross-sectional planes on the bell mouth.

(b) Tags of the points on the bell mouth (cross-sectional view of outlet). 41 points, per plane (123 total points).

Figure 2.7: Planes and points on bell mouth inlet duct

| Plane | Location (x) |
|---|---|
| Plane 1 | -0.020 m |
| Plane 2 | -0.030 m |
| Plane 3 | -0.035 m |

Table 2.3: The location of the three cross-sectional planes on the bell mouth.

A good approximation would have been to study pressure and velocity from the walls, the velocity would be zero and would start rising along the boundary layer.

For the sake of simplifying, to obtain the profiles, eight radial lines were created from each point located at 5 mm from the walls of the bell mouth.

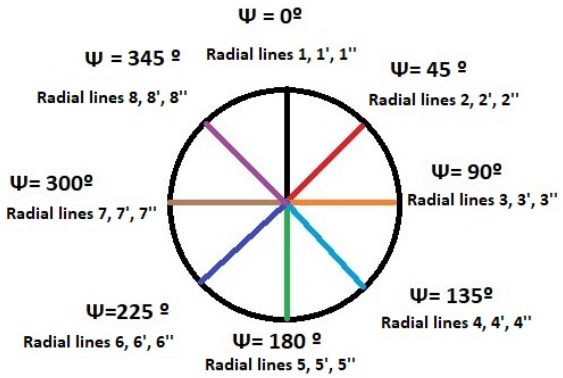


Figure 2.8: Radial lines at different ψ angles. View of the three cross-sectional planes from outlet.

### 2.7.1.. Total-Pressure profiles

Figures 2.9, 2.10, 2.11 show total-pressure profiles of cross-sections 1, 2 and 3 respectively.

#### *2.7.1.1.. Cross-section 1 (x=-0.020 m). Results of radial lines 1 to 8*

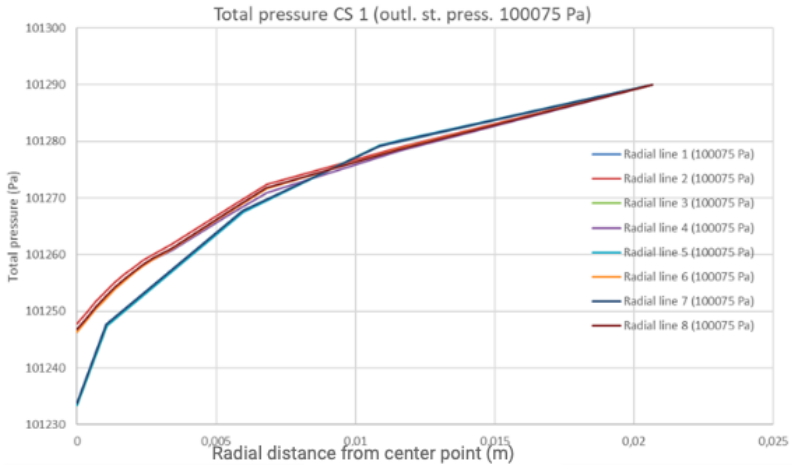


Figure 2.9: Total-pressure profile for radial lines 1 to 8 (different angles) at an outlet static pressure 100075 Pa.

#### *2.7.1.2.. Cross-section 2 (x=-0.030 m). Results of radial lines 1' to 8'*

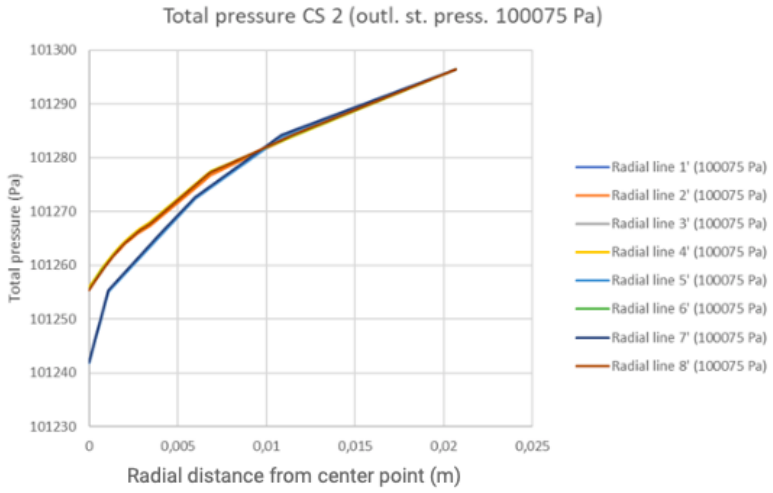


Figure 2.10: Total-pressure profile for radial lines 1' to 8' (different angles) at an outlet static pressure 100075 Pa.

*2.7.1.3.. Cross-section 3 (x=-0.035 m). Results of radial lines 1" to 8"*

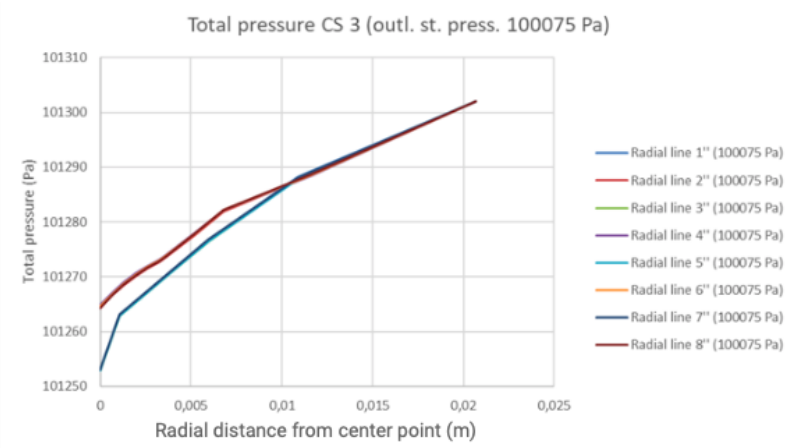


Figure 2.11: Total-pressure profile for radial lines 1" to 8" (different angles) at an outlet static pressure 100075 Pa.

## 2.7.2.. Static-pressure profiles

Figures 2.12, 2.13, 2.14 show static-pressure profiles of cross-sections 1, 2 and 3 respectively.

*2.7.2.1.. Cross-section 1 (x=-0.020 m). Results of radial lines 1 to 8*

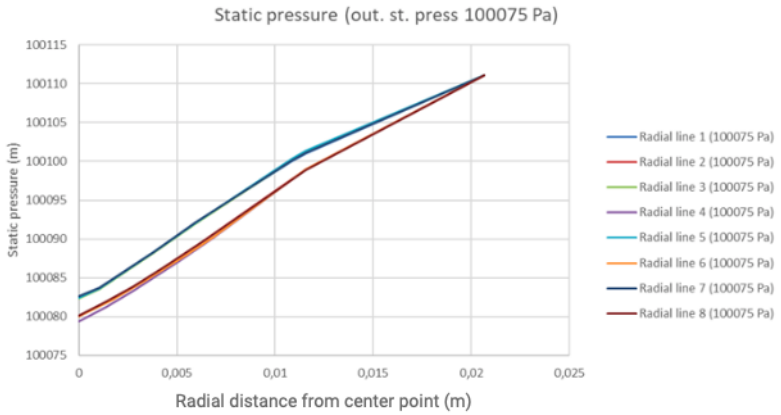


Figure 2.12: Static-pressure profile for radial lines 1 to 8 (different angles) at an outlet static pressure 100075 Pa.

*2.7.2.2.. Cross-section 2 (x=-0.030 m). Results of radial lines 1' to 8'*

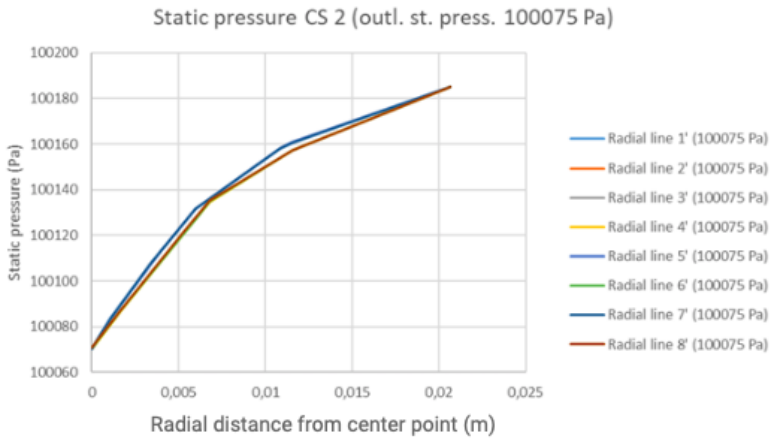


Figure 2.13: Static-pressure profile for radial lines 1' to 8' (different angles) at an outlet static pressure 100075 Pa.

*2.7.2.3.. Cross-section 3 (x=-0.035 m). Results of radial lines 1" to 8"*

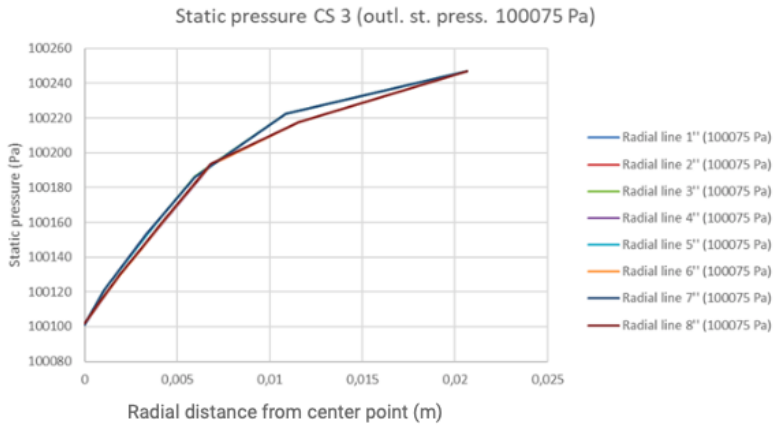


Figure 2.14: Static-pressure profile for radial lines 1" to 8" (different angles) at an outlet static pressure 100075 Pa.

### 2.7.3.. Velocity profiles

Figures 2.15, 2.16, 2.17 show velocity profiles of cross-sections 1, 2 and 3 respectively.

#### *2.7.3.1.. Cross-section 1 (x=-0.020 m). Results of radial lines 1 to 8*

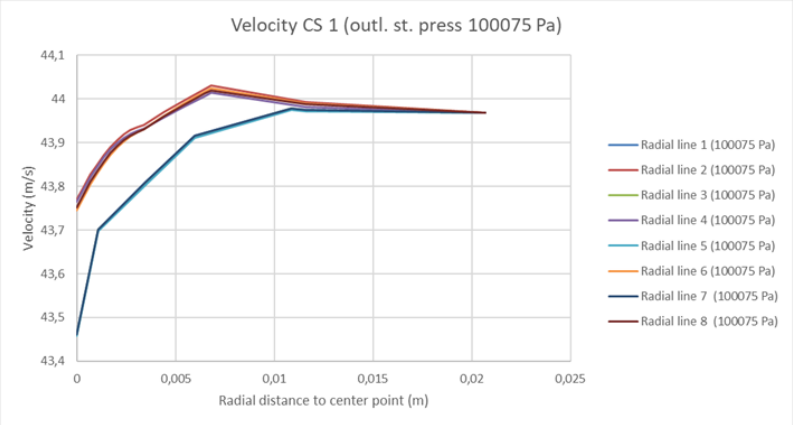


Figure 2.15: Velocity profile for radial lines 1 to 8 (different angles) at an outlet static pressure 100075 Pa.

#### *2.7.3.2.. Cross-section 2 (x=-0.030 m). Results of radial lines 1' to 8'*

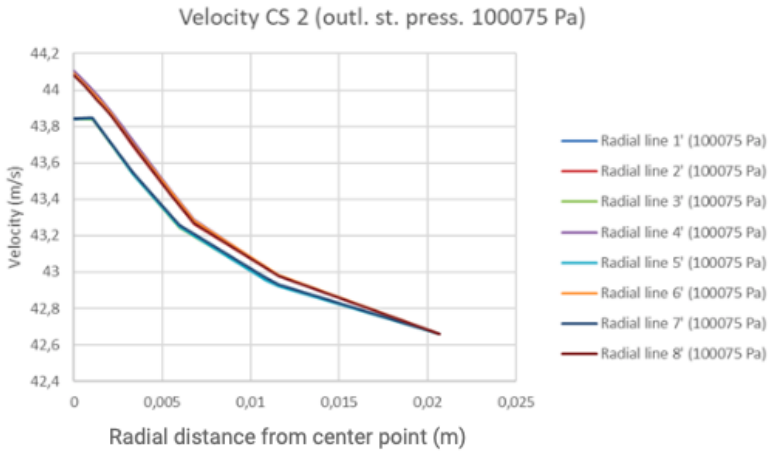


Figure 2.16: Velocity profile for radial lines 1' to 8' (different angles) at an outlet static pressure 100075 Pa.

#### *2.7.3.3.. Cross-section 3 (x=-0.035 m). Results of radial lines 1" to 8"*

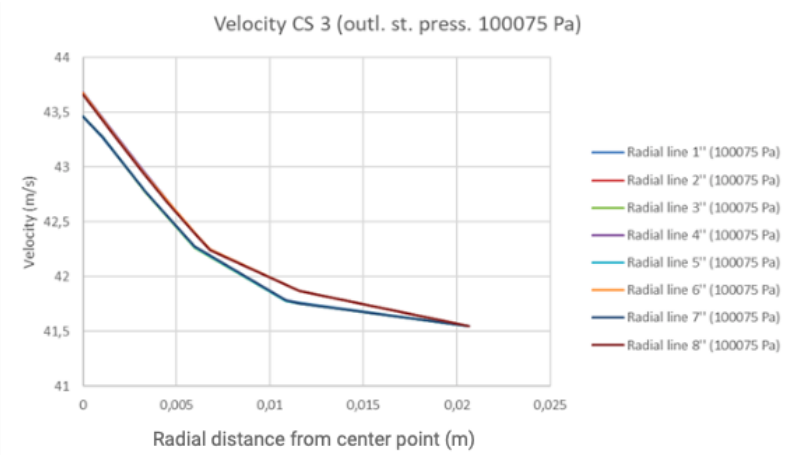


Figure 2.17: Velocity profile for radial lines 1" to 8" (different angles) at an outlet static pressure 100075 Pa.

### 2.7.4.. Comments on plots results

#### *2.7.4.1.. Total and static pressures*

Regarding total-pressure profiles at cross-section 3 and 2: something interesting is that the values of total pressure corresponding to radial lines at $0^o$, $90^o$, $180^o$ and $270^o$ (this is radial line 1, radial line 3, radial line 5 and radial line 7) have almost the same values of total pressure along them; and the values of total pressure corresponding to radial lines 2 ($45^o$), 4 ($135^o$), 6 ($225^o$) and 8 ($315^o$) have almost the same values .

More concretely, the radial lines 1 and 7 show the same values of pressure (same tendency); radial lines 2 and 8 show the same values of pressure and tendency; radial lines 3 and 5 the same values and tendency; and radial line 4 and 6 the same.

But in cross-section 1, odd radial lines keep the same tendency, but not the even ones. In this section, radial lines 2 and 8 does not shoe the same tendency (although the values are very similar). Now, radial lines 2 and 4 show the same tendency (not exactly the same, but similar) and with radial lines 6 and 8 occurs the same.

In general, there is not a big difference between plots of total-pressure in cross-sections 3, 2 and 1. The big difference is just the values of total pressure that between cross-sections tend to decrease as the flow is flowing through the duct along x axis (the values of total pressure at points on cross-section 1 are lower than in cross-section 2, and the biggest of all three cross-sections are found on cross-section 3).

Regarding static-pressure profiles: in cross-section 3 and 2 the behavior of static pressure on radial lines is kept the same as in the case of total-pressure. Radial lines 1 and 7 show same tendency; 3 and 5 the same values and tendency; and 4 and 6 the same. As in the case of total pressure.

And the same applies with cross-section 1, the tendency of the radial lines is the same as in static pressure for cross-sections 3 and 2. The main difference between static pressure

and total pressure in cross-section 1, is that the tendency of radial lines are the same as cross-sections 3 and 2. Studying the radial lines, the total pressure and static pressure tend to increase as approaching to the center point of the bell mouth. Look tables C.1, C.2, C.3, C.4, C.5.

The static pressure and dynamic pressure tends to decrease as the flow crosses the bell mouth, hence, it is normal that the total pressure decreases. This has sense since velocity has to increase as the flow is approaching to the bell mouth's outlet. Look table

The total-pressure variations are greater from cross-section 3 to 2 ( 10 Pa more or less), than from cross-section 2 to 1 ($\sim$ 5 Pa). And this is repeated on the points at different cross-sections.

Regarding the static-pressure variations, as the velocity of the flow tends to increase, it is expected that static pressure also decreases, which is something that occurs. But in the cross-sections studied, something interesting that we can see is that static pressure in cross-section 2 are lower that in cross-section 1, which is non expected since velocity should increase as approaching to outlet.

#### *2.7.4.2.. Velocity*

And now regarding velocity profiles: in cross-section 3 and 2, the velocity values tend to irease gradually as approaching to the center. In cross-section 3, the first point (5 mm from walls) has a velocity value of 41.54 m/s while at the center point the value of velocity is 43.66 m/s. In cross-section 2, the first point (5 mm from walls) has a velocity of 42.66 m/s, while at the center point the value of velocity is 44.07 m/s.

In cross-section 1, the results are a little bit different:

The radial line 2 is the one with highest values of velocity along the radial line, then number 6, number 8 and finally number 4. And the tendency is the same on these lines.

Then, from the point at 6.8 mm, the value of velocity tend to increase until the center point in which the values of velocity are 43.97 m/s.

Regarding radial lines 1, 3, 5 and 7: the velocity tend to increase from the first point studied on radial lines (5 mm from walls) to a point located at 11.5 mm. The values of velocity at that point are 43.96 m/s. Then the velocity is kept almost constant (in the center point the velocity is 43.97 m/s).

The velocity tends to increase as the fluid is crossing the bell mouth, this explains why the values of velocity are bigger as the flow is crossing the cross-sections.

#### *2.7.4.3.. Density*

As the fluid is incompressible, the density values are almost the same (insignificant differences).

### 2.7.5.. Air mass flow computation

The air mass flow computation has been done at the three cross-sections 1 to 3, and also at the inlet and outlet. Different outlet static pressures have been imposed (the total pressure has been kept constant at 1 atm) to compute the air mass flow at different velocities.

For achieving it, a dummy surface has been created. The dummy surface is a surface that is created in order to assess the air mass flow that cross the particular surface (because of the definition of air mass flow). All three surfaces are the cross-sectional areas of the bell mouth inlet duct.

An integration of the velocity profiles was needed for it, and the software allowed us to do it.

In the nexts tables 2.4 and 2.5 we can see the air mass flow computation results.

The air mass flow tends to increase as the air is flowing through the duct because the static pressure and total pressure tend to a lower value. This is because the static pressure is inversely proportional to air velocity, and the air mass flow is at the same time proportional to air velocity.

For each outlet static pressure, we can see at the different cross-sections that the air mass flow rate is higher or lower and that although the flow increases the velocity as flowing through the duct, values of air mass flow rates are not increasing. This is because the cross-sections have higher or lower values of density, influencing the value of the air mass flow rate (the surface areas are the same for cross-sections 1 to 3, look table 2.6) For example, inlet section has a value of density of 1.22 Kg/$m^3$ while cross-section 3 has 1.21 Kg/$m^3$

| Outlet Static pressure | Location | Air mass flow rate |
|---|---|---|
| 100075 Pa | Inlet | 0.0185 Kg/s |
| | Cross-section 3 | 0.0977 Kg/s |
| | Cross-section 2 | 0.0969 Kg/s |
| | Cross-section 1 | 0.0971 Kg/s |
| | outlet | 0.1036 Kg/s |
| 99500 Pa | Inlet | 0.0224 Kg/s |
| | Cross-section 3 | 0.1161 Kg/s |
| | Cross-section 2 | 0.1151 Kg/s |
| | Cross-section 1 | 0.1154 Kg/s |
| | outlet | 0.1250 Kg/s |
| 98925 Pa | Inlet | 0.0313 Kg/s |
| | Cross-section 3 | 0.1318 Kg/s |
| | Cross-section 2 | 0.1307 Kg/s |
| | Cross-section 1 | 0.1310 Kg/s |
| | outlet | 0.1732 Kg/s |
| 97775 Pa | Inlet | 0.0286 Kg/s |
| | Cross-section 3 | 0.1581 Kg/s |
| | Cross-section 2 | 0.1568 Kg/s |
| | Cross-section 1 | 0.1571 Kg/s |
| | outlet | 0.1732 Kg/s |
| 96050 Pa | Inlet | 0.0381Kg/s |
| | Cross-section 3 | 0.1898 Kg/s |
| | Cross-section 2 | 0.1882 Kg/s |
| | Cross-section 1 | 0.1886 Kg/s |
| | outlet | 0.2094 Kg/s |
| 94325 Pa | Inlet | 0.0437 Kg/s |
| | Cross-section 3 | 0.2157 Kg/s |
| | Cross-section 2 | 0.2139 Kg/s |
| | Cross-section 1 | 0.2143 Kg/s |
| | outlet | 0.2392 Kg/s |
| 93175 Pa | Inlet | 0.0469 Kg/s |
| | Cross-section 3 | 0.2308 Kg/s |
| | Cross-section 2 | 0.2289 Kg/s |
| | Cross-section 1 | 0.2293 Kg/s |
| | outlet | 0.2565 Kg/s |

Table 2.4: Air mass flow rate values at different cross-sections and outlet static pressures

| Outlet Static pressure | Location | Air mass flow rate |
|---|---|---|
| 90000 Pa | Inlet | 0.0546 Kg/s |
| | Cross-section 3 | 0.2658 Kg/s |
| | Cross-section 2 | 0.2637 Kg/s |
| | Cross-section 1 | 0.2642 Kg/s |
| | outlet | 0.2971 Kg/s |
| 80000 Pa | Inlet | 0.0709 Kg/s |
| | Cross-section 3 | 0.3400 Kg/s |
| | Cross-section 2 | 0.3376 Kg/s |
| | Cross-section 1 | 0.3382 Kg/s |
| | outlet | 0.3832 Kg/s |
| 70000 Pa | Inlet | 0.0802 Kg/s |
| | Cross-section 3 | 0.3821 Kg/s |
| | Cross-section 2 | 0.3794 Kg/s |
| | Cross-section 1 | 0.3803 Kg/s |
| | outlet | 0.4322 Kg/s |
| 60000 Pa | Inlet | 0.0849 Kg/s |
| | Cross-section 3 | 0.4027 Kg/s |
| | Cross-section 2 | 0.4000 Kg/s |
| | Cross-section 1 | 0.4012 Kg/s |
| | outlet | 0.4566 Kg/s |
| 50000 Pa | Inlet | 0.0862 Kg/s |
| | Cross-section 3 | 0.4087 Kg/s |
| | Cross-section 2 | 0.4057 Kg/s |
| | Cross-section 1 | 0.4071 Kg/s |
| | outlet | 0.4639 Kg/s |

Table 2.5: Air mass flow rate values at different cross-sections and outlet static pressures

| Location | Surface area |
|---|---|
| Inlet | 0.0393 $m^2$ |
| Plane 3 | 0.0934 $m^2$ |
| Plane 2 | 0.0944 $m^2$ |
| Plane 1 | 0.0960 $m^2$ |
| Outlet | 0.0020 $m^2$ |

Table 2.6: Cross-sectional areas

# CHAPTER 3. SYSTEM OF MEASUREMENTS

This chapter deals with the design of a system of probe arrays for static and total pressure measurements for air mass flow evaluation.

In order to obtain a proper pressure reading of the air mass flow along the duct, the idea was to place the probes in relevant positions. Moreover, since the space is very reduced, the number of probes to locate have to be small.

To locate the probes, a calibration process is needed. The calibration process describe the degree of association between one variable and another. The most common statistical method is the least-squares regression, which tries to find the best curve that minimizes the sums of squares of residuals. There are a lot of models (linear, logarithmic, exponential...). In this case, a linear regression (most common type) is chosen.

The process of linear regression was done to all radial lines and to the three cross-sectional planes.

The main parameters to understand the regression are the ”correlation coefficient” which denotes the relationship between two sets of data. (r=-1 means perfect negative relationship; r=1 means perfect positive relationship). The residual values are also an important parameter because denotes the difference between the predicted value and the real value. And this is why it is very interesting to plot the residuals values against real data. Finally, the residual standard error is a measure of the average error about the regression line.

After assessing the results for the three cross-sectional sections 1, 2 and 3; the cross-section 2 was selected to be the section to locate the probes because the regression curve was more adjusted along the radial lines and the residual plots showed values nearest 0.

The total pressure regression curve was studied for radial lines 1, 3, 5 and 7 because of the symmetry of values and because the total pressure was more adjusted to predicted line (residuals more close to zero)

And static pressure regression curve was studied for radial lines 2, 4, 6 and 8 because the residuals were closer to zero than the odd radial lines.

# 3.1.. Total pressure

## 3.1.1.. Adjusted regression curve

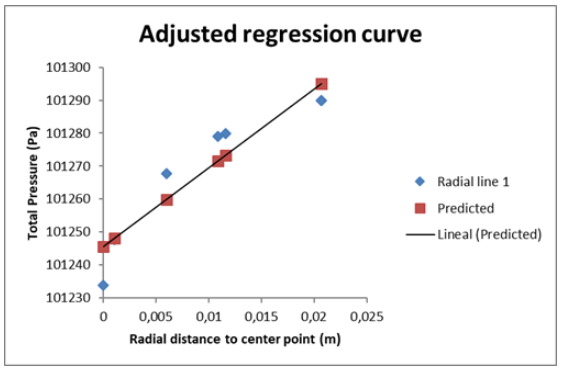


(a) Adjusted regression curve for radial line 1 (total pressure)

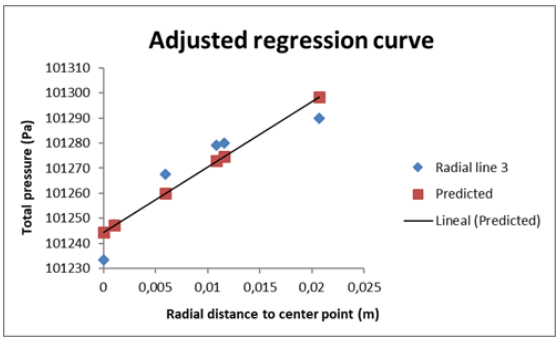


(b) Adjusted regression curve for radial line 3 (total pressure)

Figure 3.1: Adjusted regression curve for radial lines 1 and 3 (total pressure)

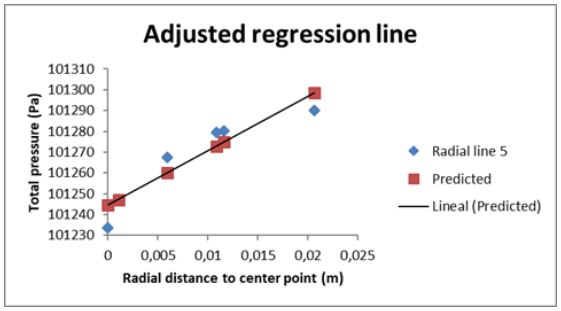


(a) Adjusted regression curve for radial line 5 (total pressure)

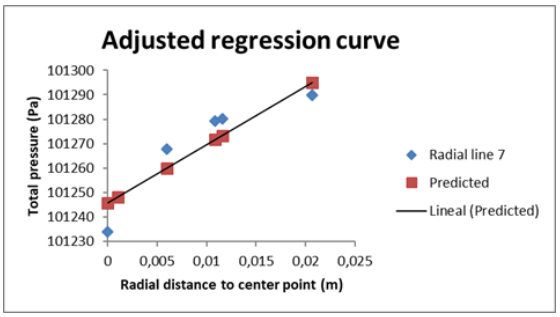


(b) Adjusted regression curve for radial line 7 (total pressure)

Figure 3.2: Adjusted regression curve for radial lines 5 and 7 (total pressure)

In figure 3.1 can be seen the regression curves for radial lines 1 and 3 (total pressure); and in figure 3.2 can be seen the regression curves for radial lines 5 and 7 (total pressure).

### 3.1.2.. Residual plots

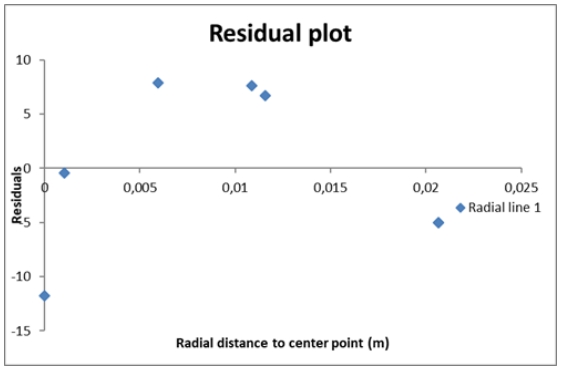


(a) Residuals plot for radial line 1 (total pressure)

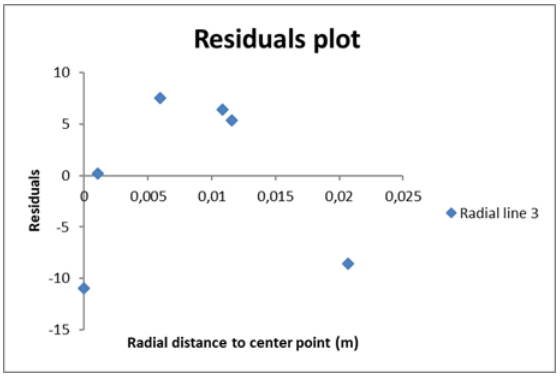


(b) Residuals plot for radial line 3 (total pressure)

Figure 3.3: Residuals plot for radial lines 1 and 3 (total pressure)

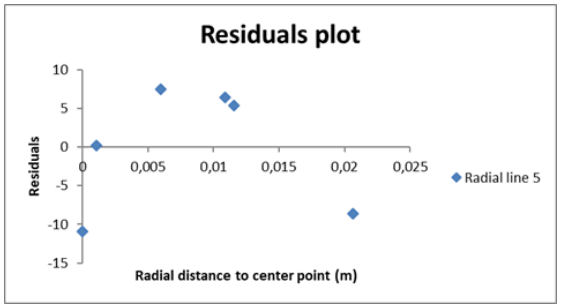


(a) Residuals plot for radial line 5 (total pressure)

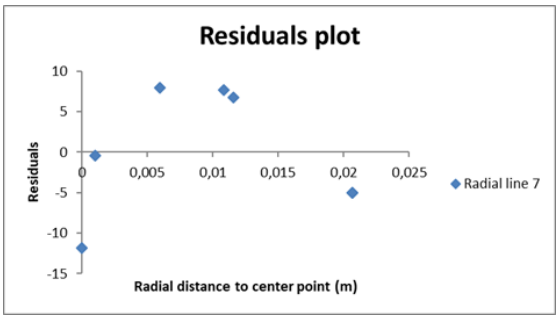


(b) Residuals plot for radial line 7 (total pressure)

Figure 3.4: Residuals plot for radial lines 5 and 7 (total pressure)

In figure 3.3 can be seen the residual plot for radial lines 1 and 3 (total pressure); and in figure 3.4 can be seen the regression plot for radial lines 5 and 7 (total pressure).

## 3.2.. Static pressure

### 3.2.1.. Adjusted regression curve

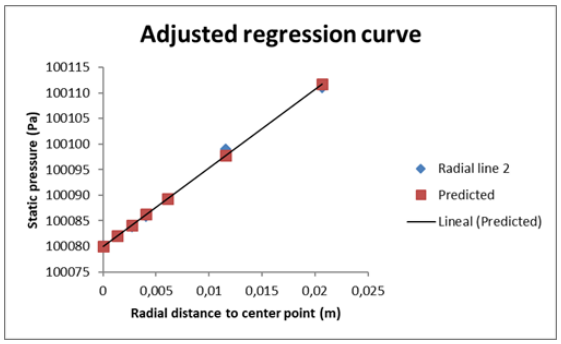


(a) Adjusted regression curve for radial line 2 (static pressure)

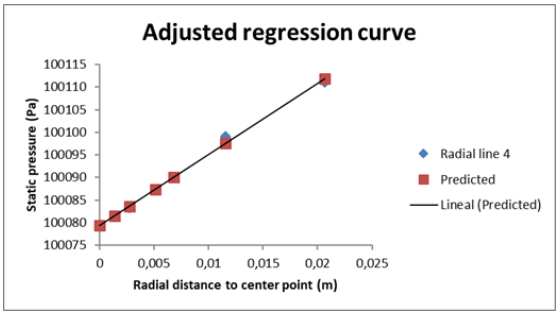


(b) Adjusted regression curve for radial line 4 (static pressure)

Figure 3.5: Adjusted regression curve for radial lines 2 and 4 (static pressure)

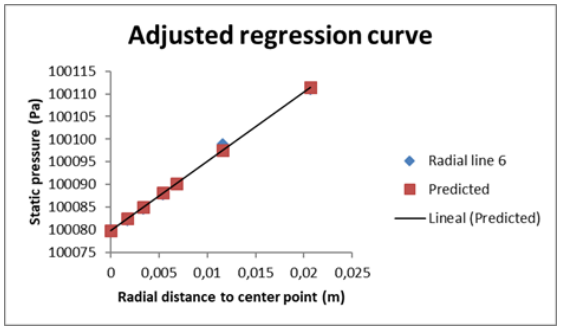


(a) Adjusted regression curve for radial line 6 (static pressure)

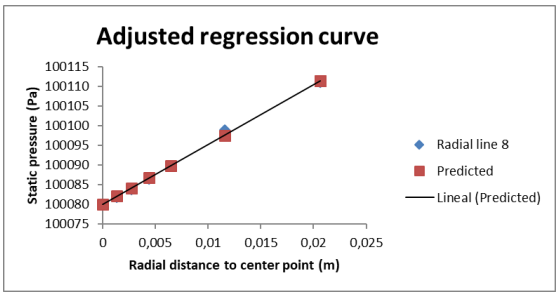


(b) Adjusted regression curve for radial line 8 (static pressure)

Figure 3.6: Adjusted regression curve for radial lines 6 and 8 (static pressure)

In figure 3.5 can be seen the regression curves for radial lines 2 and 4 (static pressure); and in figure 3.6 can be seen the regression curves for radial lines 6 and 8 (static pressure).

### 3.2.2.. Residual plots

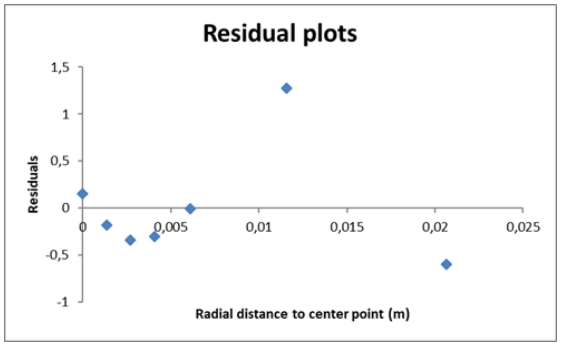


(a) Residuals plot for radial line 2 (static pressure)

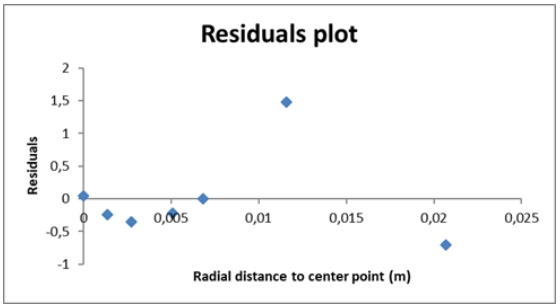


(b) Residuals plot for radial line 4 (static pressure)

Figure 3.7: Residuals plot curve for radial lines 2 and 4 (static pressure)

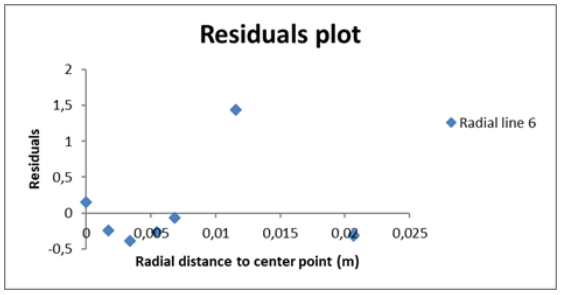


(a) Residuals plot for radial line 6 (static pressure)

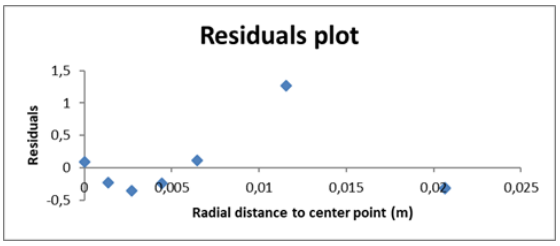


(b) Residuals plot for radial line 8 (static pressure)

Figure 3.8: Residuals plot for radial lines 6 and 8 (static pressure)

In figure 3.7 can be seen the residual plots for radial lines 2 and 4 (static pressure); and in figure 3.8 can be seen the residual plots for radial lines 6 and 8 (static pressure).

## 3.3.. Results

### 3.3.1.. Total pressure

| radial lines | correlation coefficient (r) |
|---|---|
| Radial line 1 | 0.9344 |
| Radial line 3 | 0.9295 |
| Radial line 5 | 0.9295 |
| Radial line 7 | 0.9338 |

Table 3.1: correlation coefficient (r) for radial lines 1, 3, 5, 7.

| Radial lines | Observations (order points) | Standard residuals |
|---|---|---|
| R. Line 1 | Point 1 | -1.531 |
| | Point 2 | -0.056 |
| | Point 3 | 1.027 |
| | Point 4 | 0.989 |
| | Point 5 | 0.875 |
| | Point 6 | -0.650 |
| | Point 7 | -0.653 |
| R. Line 3 | Point 1 | -1.369 |
| | Point 2 | 0.026 |
| | Point 3 | 0.940 |
| | Point 4 | 0.801 |
| | Point 5 | 0.671 |
| | Point 6 | -1.07 |
| R. Line 5 | Point 1 | -1.366 |
| | Point 2 | 0.0229 |
| | Point 3 | 0.9345 |
| | Point 4 | 0.8064 |
| | Point 5 | 0.675 |
| | Point 6 | -1.073 |
| R. Line 7 | Point 1 | -1.530 |
| | Point 2 | -0.058 |
| | Point 3 | 1.024 |
| | Point 4 | 0.992 |
| | Point 5 | 0.877 |
| | Point 6 | -0.651 |
| | Point 7 | -0.653 |

Table 3.2: Standard residuals values for radial lines 1, 3, 5, 7.

### 3.3.2.. Static pressure

| radial lines | correlation coefficient (r) |
|---|---|
| Radial line 2 | 0.9984 |
| Radial line 4 | 0.9981 |
| Radial line 6 | 0.9988 |
| Radial line 8 | 0.9990 |

Table 3.3: correlation coefficient (r) for radial lines 2, 4, 6 and 8

| Radial lines | Observations (order points) | Standard residuals |
|---|---|---|
| R. Line 2 | Point 1 | 0.2455 |
| | Point 2 | -0.299 |
| | Point 3 | -0.553 |
| | Point 4 | -0.4917 |
| | Point 5 | -0.011 |
| | Point 6 | 2.085 |
| | Point 7 | -0.975 |
| R. Line 4 | Point 1 | 0.063 |
| | Point 2 | -0.347 |
| | Point 3 | -0.504 |
| | Point 4 | -0.3128 |
| | Point 5 | 0.0039 |
| | Point 6 | 2.117 |
| | Point 7 | -1.020 |
| R. Line 6 | Point 1 | -0.252 |
| | Point 2 | -0.398 |
| | Point 3 | -0.643 |
| | Point 4 | -0.434 |
| | Point 5 | -0.107 |
| | Point 6 | 2.371 |
| | Point 7 | -0.511 |
| | Point 8 | -0.5279 |
| R. Line 8 | Point 1 | 0.1600 |
| | Point 2 | -0.433 |
| | Point 3 | -0.654 |
| | Point 4 | -0.446 |
| | Point 5 | 0.200 |
| | Point 6 | 2.33 |
| | Point 7 | -0.564 |
| | Point 8 | -0.595 |

Table 3.4: Standard residuals values for radial lines 2, 4, 6, 8.

## 3.4.. Location of the probes on the bell mouth inlet duct

A very finite number of points were selected because the working area of the bell mouth is very narrow (less than 10 mm, so there cannot be placed a high number of probes).

So the final election of the points was based on those points with a less value of standard error.

For total-pressure probes, figure 3.3 and figure 3.4 showed that the point at 0.0010 mm (this is, from the wall at 5 mm) is the most closed to the reference line (predicted). Also, the point at the center point (25 mm from the walls) is one with less standard error deviation in (radial lines 1 and 7). And finally, one more point was selected, the one at 12 mm (17 mm from the walls). Since there is symmetry on the radial lines, in just one radial line the probes were located (radial line 1) and at the corresponding position.

For static-pressure probes, the figure 3.7 and figure 3.8 showed that the point at 5 mm (this is, from the wall at 10 mm) is the most closed to the reference line (predicted). It was selected as the position to locate the static-pressure probes on the four radial lines (there is symmetry also).

The instrumentation chosen regarding static and total pressure are: four wall-static pressure orifices, total-pressure probes (rake of 2) and a total-pressure probe at the center point.

All located in the plane at 30 mm from outlet. In figure 3.9 the position of total-pressure and static-pressure probes is detailed. In blue colour, the four wall-static pressure orifices. In green colour, the total-pressure probes.

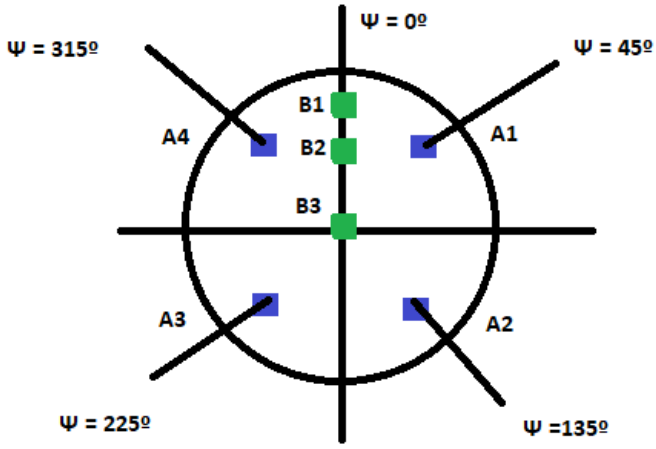


Figure 3.9: Frontal view of the bell mouth. With the position of total and static-pressure probes at 30 mm from outlet. In blue, four wall-static pressure orifices. In green, three total-pressure probes.

To sum up all results, all results are introduced in a tables. The summary of positions of the two total-pressure rake probes are in table 3.5

The position of the total-pressure probe is shown in table 3.6

The summary of the positions of the four wall-static probes are in table 3.7

| Total-pressure rake identification | $\psi$ angle | Radial distance (from wall) |
|---|---|---|
| B1 | $0^o$ | 5 mm |
| B2 | $0^o$ | 17 mm |

Table 3.5: Positions of the two total-pressure rake probes

| Total-pressure probe identification | $\psi$ angle | radial distance from wall |
|---|---|---|
| B3 | $0^o$ | 25 mm |

Table 3.6: Position of the total-pressure probe

| Static-pressure probe identification | $\psi$ angle | Radial distance from wall |
|---|---|---|
| A1 | $45^o$ | 5 mm |
| A2 | $135^o$ | 5 mm |
| A3 | $225^o$ | 5 mm |
| A4 | $315^o$ | 5 mm |

Table 3.7: Positions of the four static-pressure probes

## 3.5.. Measurement devices

### 3.5.1.. Total and static pressure measurement devices

For total and static pressure measurements, the devices chosen were pressure transducers. The Paroscientific Digiquarz [10] transducers have been selected because of the advantage of being fully calibrated and with crystal frequency outputs. There exist pressure transducers called ”Series 2000”, ”Series 3000” and ”Series 4000”. However, the pressure transducers used in Aerospace field are the ”Series 2000”. The other transducers are used in other fields, like metrology, Oceanography, Energy Exploration...

Moreover, these transducers (”Series 2000”) work in 10 absolute pressure ranges and 7 gauge pressure ranges. One of these absolute pressure ranges wide from 0 psi (0 Pa) to 23 psi (0.16 MPa), so being within the range of the studied pressures. Regarding the 7 gauge pressure ranges, one of these wide from 0 psi (0 Pa) to 22 psi (0.15 MPa), also within the studied pressures’ range. This is why the chosen pressure transducers are the Paroscientific Digiquarz Series 2000.

The ”Series 2000” transducers work with a 0.01 % typical accuracy (high accuracy). They Are fully calibrated and have high stability and reliability. In addition, are characterized by a low consumption [11]. Look in Annex E.1.

The reading of pressure data taken with the pressure transducers will be done with a digital electronic pressure indicator Paroscientific model 735. More information at Annex E.2.

The two total-pressure rake probes can be measured with a digital manometer (Hti-Xintai). Look Annex E.3.

# CHAPTER 4. BUDGET FOR CONSTRUCTION AND ASSEMBLY

In this chapter, a budget is drawn up. Aspects as the creation of the bell mouth, the costs of the simulation program and the costs of pressure and temperature probes for measuring the air mass flow are covered.

## 4.1.. Materials' analysis for creating the bell mouth

There are several materials that can be used for the construction of the bell mouth inlet duct.

In general, the aviation Industry use Aluminum, Steel (stainless) or composite materials (Fiberglass Carbon fiber, Kevlar ...). [18]

The use of one material or another depends on the price willing to pay and the quality that is sought. In general, composite materials have better quality in terms of properties. The main problem is the price, they are usually more expensive materials than aluminum or steel.

To determine which material we must choose to create our bell mouth, we have to analyze the quality (physical properties) and the price.

The properties analyzed include:

Young's Modulus: which measures the stiffness capacity of the material. It defines the relation between stress and deformation of the material.

Shear Modulus: also called the rigidity modulus. Defined as the ratio between shear stress and shear strain, this is, the ratio of shear stress per unit length. [19] [20].

Poisson ratio: is the ratio of the relative contraction strain (normal, cross-sectional or lateral) normal to the applied load to the axial strain in the direction of the applied load. [21]

Tensile strength: it is the maximum load of stress that a material can withstand being stretched before breaking. [22]

Coefficient of thermal expansion: it describes how the size of an object changes with a change in temperature. [23]

The properties of aluminium alloys and stainless steel are shown in table 4.1. Note that are approximate values for aluminium alloys and stainless teel, because there are litte differences in properties between some kind of alloys and others.

Regarding composite materials, in table 4.2 the main properties are shown.

| Properties | Aluminium alloys | Stainless steel |
|---|---|---|
| Young Modulus E | $\sim$ 70 GPa | $\sim$ 189 GPa |
| Shear Modulus G | $\sim$ 26 GPa | $\sim$ 74.1 GPa |
| Poisson Ratio $\nu$ | $\sim$ 0.3 | $\sim$ 0.28 |
| Tensile strength $\sigma$ | ($\sim$ 0.25, $\sim$ 0.5) GPa | $\sim$ 0.8 GPa |
| Density $\rho$ | $\sim$ 2.8 mg/$m^3$ | $\sim$ 7.8 mg/$m^3$ |
| Coefficient of linear thermal expansion $\alpha$ | $\sim$ 23 x $10^{-6}$ | $\sim$ 12 x $10^{-6}$ |

Table 4.1: Properties of the aluminium alloys and stainless steel [15] [16]

| Properties | HR Carbon/epoxy | Kevlar/epoxy | R Glass/epoxy |
|---|---|---|---|
| Young Modulus E | 130 GPa | 75 GPa | 53 GPa |
| Density $\rho$ | 1.5 x $10^9$ mg/$m^3$ | 1.37 x $10^9$ mg/$m^3$ | 2 x $10^9$ mg/$m^3$ |
| Tensile strength $\sigma$ | $\sim$ 1.2 GPa | $\sim$ 1.5 GPa | $\sim$ 1.9 GPa |
| Linear therm. exp. coeff. $\alpha$ | $\sim$ 35 x $10^{-6}$ | $\sim$ 60 x $10^{-6}$ | $\sim$ 31 x $10^{-6}$ |

Table 4.2: Properties of composites HR Carbon/epoxy; Kevlar/epoxy and R Glass/epoxy [17]

The Young's Modulus play an important role in terms of structural deformation. A higher value, implies that the structure will be less prone to warp and break. As we can see, the Stainless steel is the material with highest Young's modulus. The composites in general have also great values, but the R glass with epoxy resin shows the lowest value.

Regarding the tensile strength, the highest values are shown by composites. The HR Carbon with epoxy resin is the one with lowest value among the other composites shown in table 4.2. This is, it has 130GPa of young modulus E but only approx. 1.2 GPa of tensile strength is able to support before breaking. The Kevlar with epoxy resin has a lower value of Young's Modulus but it can support highest value of tensile strength. And the composite with highest capacity of supporting tensile strength is R glass with epoxy resin, with approximately 1.9 GPa.

The aluminium alloys and stainless steel have different behavior in the sense that the stainless steel has the highest value of Young's modulus but also the tensile strength that can support before breaking is higher too.

Regarding the thermal expansion coefficient, it will not play an important role because in fact the temperatures during the rig test will not be really high (in fact, ambient temperatures). Nevertheless, the highest value corresponds to Kevlar with epoxy resin and the lowest to stainless steel.

The cost is an important factor when it comes the choice of a material or another. The composite materials are expensive although the mechanical properties are slightly better. However, the aluminum alloys and stainless steel have more competitive prices, this is why the final choice relied in aluminium alloys and stainless steel.

Comparing aluminium alloys and stainless steel, the final choice was aluminium alloys because they are less dense than stainless steel.

There are several aluminum alloys: series 1000, series 2000, series 3000, series 4000, series 5000, series 6000 and series 7000.

After comparing the series, series 5000 and series 6000 showed a similar behavior, but as the 6061 aluminium alloys (series 6000) have good mechanical properties and are very common for general purpose, the final election was that. Properties shown in table 4.3

| **Properties** | **6061 Aluminium alloy** |
|---|---|
| Young Modulus E | 68.9 GPa |
| Poisson Ratio ν | 0.33 |
| Tensile strength σ | ($\sim$ 0.12, $\sim$ 0.29) GPa |
| Density ρ | 2.70 x $10^9$ mg/$m^3$ |
| Coefficient of linear thermal expansion α | 23 x $10^{-6}$ |

Table 4.3: Properties of 6061 aluminium alloy [24]

A good election could have been also nylon or fiberglass.

## 4.2.. Economical impact

For the economical cost of the project, the pressure probes price, the material cost for creating the bell mouth and the salary for a Junior Engineer for all the project work were taken into account.

The next table shows the price of the corresponding item. Regarding the probes, the total sum was taken into account, not the individual price. Is worth to say that the price of the probes is roughly estimated and the import price must be taken into account, although it not appears in the next table.

Regarding the duct, a budget for the bell mouth construction was asked to a factory. The materials chosen were aluminum 6061 and nylon. The corresponding price has been 360 euros for an individual piece if considering aluminum, and 250 if considering nylon . In the annex F the complete budget for the bell mouth is attached.

Finally, the payment to a Junior Engineer at 15 euros/hour, with a total sum of 450 hours of work, corresponds a total of 6750 euros.

| Item | Price |
|---|---|
| Absolute and gauge pressure transducer | 6292 € |
| 735 intelligent display | 3617.90 € |
| three total-pressure rake | 400 € |
| Digital manometer | 31.15 € |
| Total-pressure probe (1 unit) | 4.3 € |
| Wall-static pressure probes (4 units) | 71 € |
| Nylon Bell mouth inlet duct | 250 € |
| Aluminum 6061 Bell mouth inlet duct | 360 € |
| Junior Engineer work | 6750 € |
| **Total price sum (Alum. bell mouth)** | **17526.35 €** |
| **Total price sum (Nylon bell mouth)** | **17416.35 €** |

Table 4.4: Total price sum of the necessary items for the project

Note: it is important to remark that the price of the total sum may vary taking into account the import price. Therefore, this table shows an approximation of the total cost of the products.

## 4.3.. Future work

For the future work, it has to be verified that the positions of the probes to measure the air mass flow have been done correctly, measuring it experimentally.

The project about the EvoJet B170 Neo is going to be continued by the students of EETAC (UPC Castelldefels).

# CONCLUSIONS

The aim of this project was to review alternative solutions for adapting the air flow and assessing the air massflow into a micro gas turbine engine in ground testing conditions (EvoJet B170 Neo) and to design a scalable air intake that provides optimal performance and accurate measurements.

On the literature review, the importance and types of test facilities for aerospace industries are explained. Moreover, why the use of bell mouth inlet ducts and the purpose of them, has been exposed. It is clear that this type of ducts allows the air flow to be funneled so that it enters without distortion in the engine, and when conditioned, the measurements are not affected by any distortion or vortex effects. These ducts, enable accurate airflow measurement during on-ground rig testing.

In addition, an analysis with CFD tool has been done. Firstly, three different bell mouth inlet ducts have been designed with CAD software. Then, it was important to establish adequate boundary conditions to solve the problem properly (solve the problem with the on-ground conditions). Also, it was important to establish an adequate trade-off between quality of the results and accuracy (the higher number of mesh elements, the more computational effort), so it was necessary to choose a good level of refinement of the meshes to obtain reasonable results in a brief period of time.

Regarding the results, they were obtained for the three bell mouths at an outlet static pressure of 100075 Pa. Since the bell mouth inlet duct 1 showed a good performance (based on streamlines, velocity contours, pressure contours, and its values), it was chosen as a good bell mouth for the EvoJet B170 Neo. Then, this bell mouth was studied at different velocities by generating pressure gradients between inlet and outlet. Three different cross-sections have been studied (located at -0.020 mm, -0.030 mm and -0.035 mm from outlet, respectively). To do it, eight radial lines were located at the cross-sections, and total and static pressure profiles, as well as velocity profiles, were obtained. In addition, the air mass flow rates at the different cross-sections and pressure gradients were obtained.

Regarding the location of the probes, it was needed a calibration (linear regression) to know which was the most suitable place. Four static wall pressure probes, a rake of two total-pressure probes and a total pressure probe (center point) is the instrumentation needed to continue with the EvoJet B170 Neo project. The exact position of them have been represented and wrote in table format. Also, the equipment and the data sheet have been added in the annex.

Finally, the last part of the project has consisted on an assembly and commissioning budget. First, the properties and prices of a series of materials have been analyzed, and it has been considered that aluminum 6061 is the most suitable material for creating the bell mouth inlet duct. Since it is not as expensive as composites materials and also because it can withstand the tests (it does not deform easily and is quite light). A Galician company has been contacted in order to ask for a budget for the bell mouth inlet duct, both in aluminum 6061 and nylon. An individual bell mouth of these dimensions, cost a total of 360 euros in the case of aluminum 6061, and 250 euros in the case of nylon.

The total cost of the project, considering the measuring equipment, the bell mouth and a payment to a junior engineer has been added to the budget. The total cost of the project is 17526.35 euros with the aluminum bellmouth or 17416.35 euros with the nylon bell mouth.

This project is a preliminary design, the bell mouth is not built yet.

# BIBLIOGRAPHY


[1] Soares Claire. *Gas Turbines: A Handbook of Air, Land and Sea Applications*. ID: IN-09788 7, 8, 12, 13, 14

[2] R. Jacques. Operation and performance measurement on engines in sea level test facilities, 1984.[Figure] AGARD Lecture Series No.132. xi, xi, xi, 8, 9, 11, 13, 15

[3] P.P. Walsh, P. Fletcher. *Gas Turbine performance*.Second edition. 2004. Blackwell Science Ltd. xi, xi, 13, 14, 15, 16

[4] D.J. Lahti. *Discharge Coefficient of a Sub-Critical Flow Meter*. DTIC Selected. September 1990. 15

[5] Kian Cheong Lim, Arianne Nartyasari Michael Tavares, Yiyan Wang. *Air mass flow rate measurement* 15

[6] SAE ARP 741 *Gas Turbine Engine Test Cell Correlation*. March 1976. 11

[7] Brix, Neuwerth, Jacob. *The inlet-vortex system of jet engines operating near the ground*. AIAA-2000-3998. 2000. xi, 12

[8] https://www.solidworks.com/product/solidworks-flow-simulation 19

[9] Blair, Cahoon. *Best Bell* http://www.profblairandassociates.com/pdfs/RET_bell mouth_Sept.pdf 20

[10] http://paroscientific.com/products.php 51

[11] http://www.mercan.co.jp/model216b.pdf xiii, xiii, xv, xv, 51, 95, 96, 97

[12] https://uk.rs-online.com/web/p/thermocouples/1104482/

[13] https://www.picotech.com/data-logger/tc-08/usb-tc-08-specifications

[14] Smith, Stephen. *Airflow Calibration of a bell mouth Inlet for Measurement of Compressor Airflow in Turbine-powered Propulsion Simulators*

[15] J. E. Gordon, *Estructuras, o porqué las cosas no se caen* , ed.Calamar, 2004 xv, 54

[16] Engineering ToolBox, (2005). Thermal Expansion of Metals. [online] Available at: https://www.engineeringtoolbox.com/thermal-expansion-metals-d_859.html [13 July. 2019]. xv, 54

[17] Schwartz, Mel. *Innovations in Materials Manufacturing, Fabrication, and Environmental Safety* xv, 54

[18] Celtech Corporation. [online]: https://celtech.com/engine-support-equipment-overview/bell mouths/ [13 July. 2019] 53

[19] Engineering ToolBox, (2005). Modulus of Rigidity. [online] Available at: https://www.engineeringtoolbox.com/modulus-rigidity-d_946.html [13 July 2019]. 53

[20] IUPAC, *Compendium of Chemical Terminology* , 2nd ed. (1997) 53

[21] Engineering ToolBox, (2008). Poisson's ratio. [online] Available at: https://www.engineeringtoolbox.com/poissons-ratio-d_1224.html [13 July 2019]. 53

[22] Giancoli, Douglas. *Physics for Scientists and Engineers*. Third Edition (2000). 53

[23] Engineering ToolBox, (2003). Coefficients of Linear Thermal Expansion. [online] Available at: https://www.engineeringtoolbox.com/linear-expansion-coefficients-d_95.html [13 July 2019]. 53

[24] ASM International, *Properties of Wrought Aluminum and Aluminum Alloys: 6061* 1990, p. 102-103. xv, 55

[25] https://www.thermocoupleinfo.com/thermocouple-types.htm

[26] http://paroscientific.com/pdf/D100_Accessories.pdf xiii, 98

[27] https://hti-instrument.com/products/ht-1890-manometer xiii, 100

# APPENDICES

# APPENDIX A. FIRST BELLMOUTH DESIGNED RESULTS

The pressure contour is shown in figure A.1.

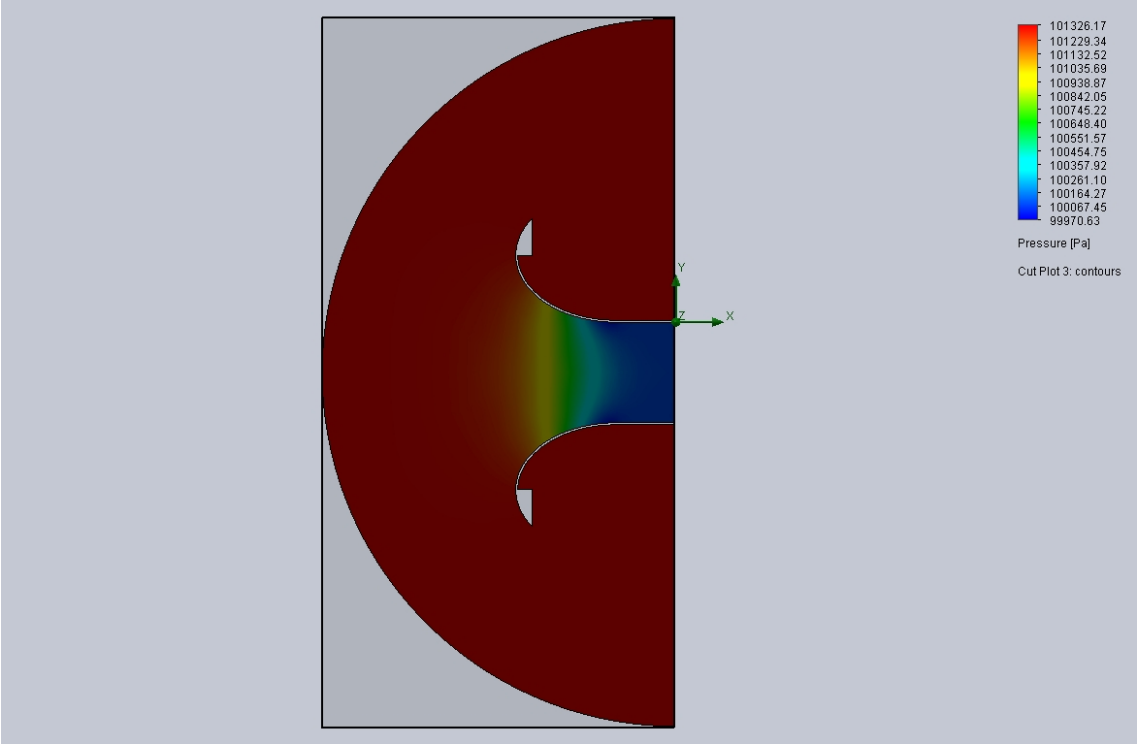


Figure A.1: Pressure contour for the first bell mouth

The velocity contour is shown in figure A.2.

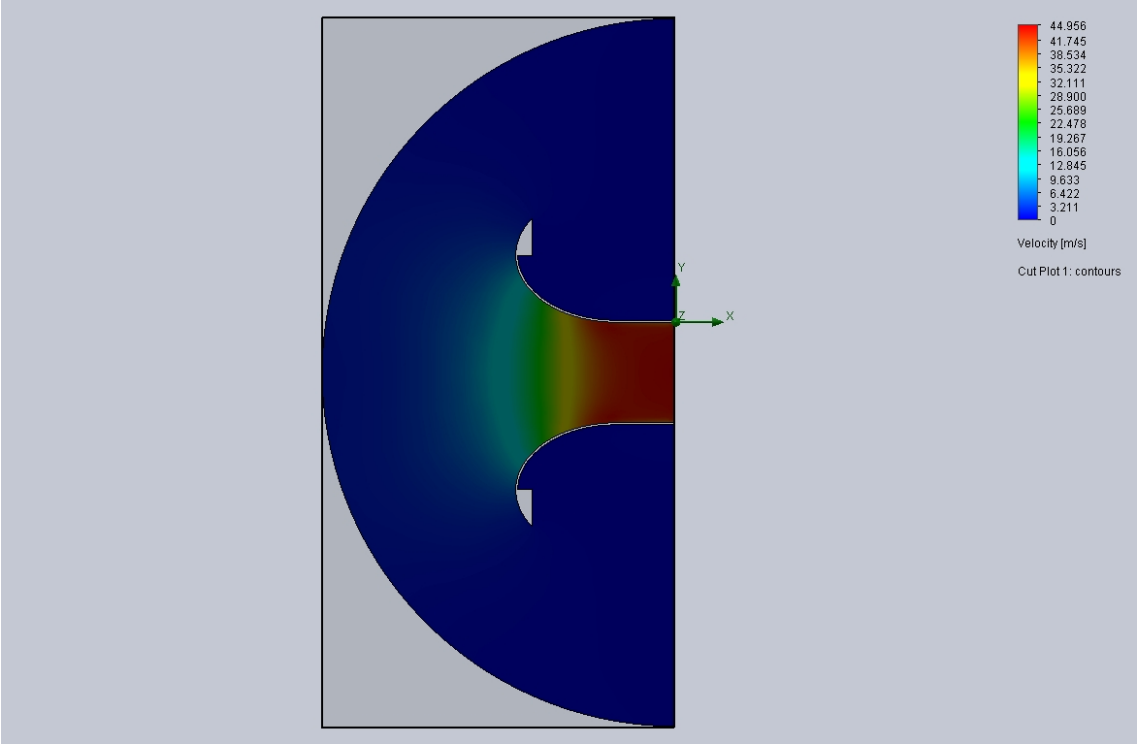


Figure A.2: Velocity contour for the first bell mouth

The streamlines are shown in figure A.3.

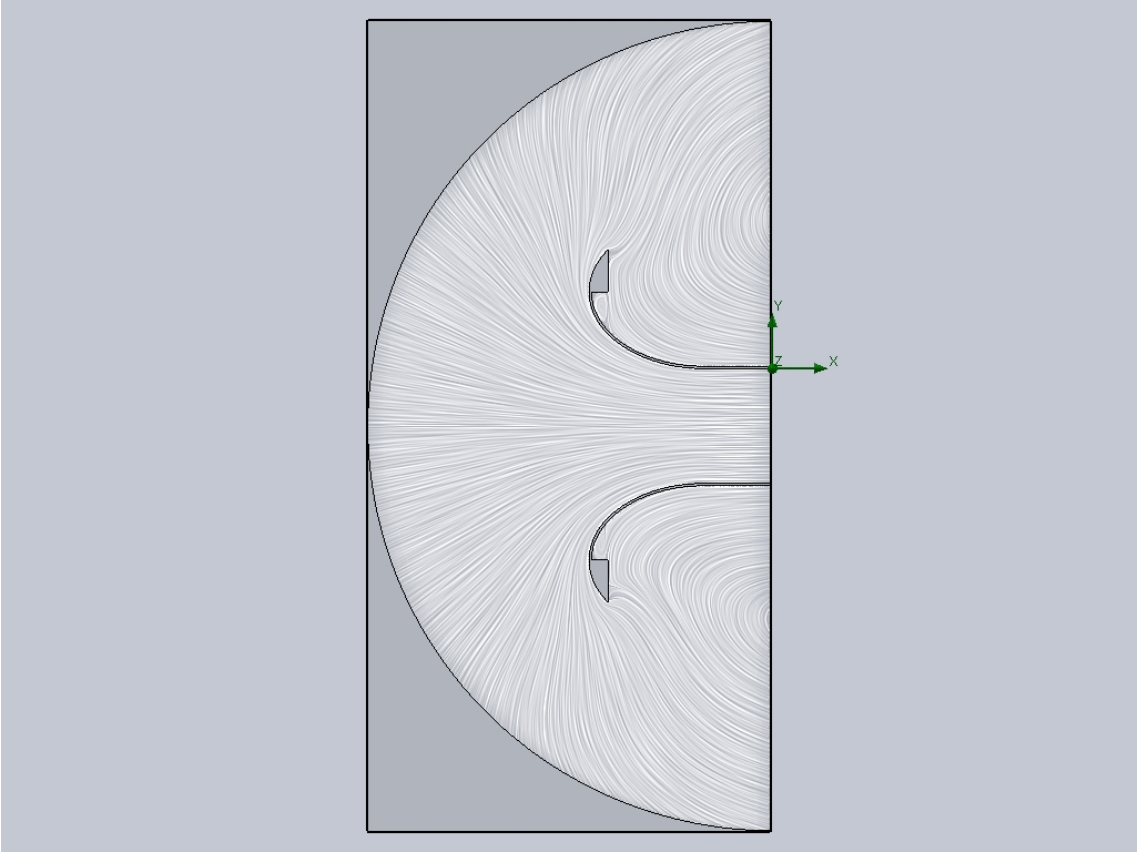


Figure A.3: Streamlines entering the first bell mouth

# APPENDIX B. NAME, AND POSITION OF THE POINTS ON THE FOUR PLANES

| Curves | Planes (y=0 m; z=0 m) | Points | Coordinate y | Coordinate z |
|---|---|---|---|---|
| Curve 2 (A) | Plane 1 | Point 1 | -0.005 m | 0 m |
| | Plane 2 | Point 2 | -0.004 m | 0 m |
| | Plane 3 | Point 3 | -0.005 m | 0 m |
| | Plane 4 | Point 4 | -0.005 m | 0 m |
| Curve 3 (B) | Plane 1 | Point 5 | -0.009 m | -0.012 m |
| | Plane 2 | Point 6 | -0.008 m | -0.012 m |
| | Plane 3 | Point 7 | -0.008 m | -0.012 m |
| | Plane 4 | Point 8 | -0.009 m | -0.012 m |
| Curve 4 (C) | Plane 1 | Point 9 | -0.019 m | -0.019 m |
| | Plane 2 | Point 10 | -0.019 m | -0.020 m |
| | Plane 3 | Point 11 | -0.019 m | -0.019 m |
| | Plane 4 | Point 12 | -0.019 m | -0.019 m |
| Curve 5 (D) | Plane 1 | Point 13 | -0.031 m | -0.019 m |
| | Plane 2 | Point 14 | -0.031 m | -0.020 m |
| | Plane 3 | Point 15 | -0.031 m | -0.019 m |
| | Plane 4 | Point 16 | -0.031 m | -0.019 m |
| Curve 6 (E) | Plane 1 | Point 17 | -0.041 m | -0.012 m |
| | Plane 2 | Point 18 | -0.042 m | -0.012 m |
| | Plane 3 | Point 19 | -0.041 m | -0.012 m |
| | Plane 4 | Point 20 | -0.041 m | -0.012 m |
| Curve 7 (F) | Plane 1 | Point 21 | -0.045 m | 0 m |
| | Plane 2 | Point 22 | -0.046 m | 0 m |
| | Plane 3 | Point 23 | -0.045 m | 0 m |
| | Plane 4 | Point 24 | -0.045 m | 0 m |
| Curve 8 (G) | Plane 1 | Point 25 | -0.041 m | 0.012 m |
| | Plane 2 | Point 26 | -0.042 m | 0.012 m |
| | Plane 3 | Point 27 | -0.041 m | 0.012 m |
| | Plane 4 | Point 28 | -0.041 m | 0.012 m |
| Curve 9 (H) | Plane 1 | Point 29 | -0.031 m | 0.019 m |
| | Plane 2 | Point 30 | -0.031 m | 0.020 m |
| | Plane 3 | Point 31 | -0.031 m | 0.019 m |
| | Plane 4 | Point 32 | -0.031 m | 0.019 m |
| Curve 10 (I) | Plane 1 | Point 33 | -0.019 m | 0.019 m |
| | Plane 2 | Point 34 | -0.019 m | 0.020 m |
| | Plane 3 | Point 35 | -0.019 m | 0.019 m |
| | Plane 4 | Point 36 | -0.019 m | 0.019 m |
| Curve 11 (J) | Plane 1 | Point 37 | -0.009 m | 0.012 m |
| | Plane 2 | Point 38 | -0.008 m | 0.012 m |
| | Plane 3 | Point 39 | -0.009 m | 0.012 m |
| | Plane 4 | Point 40 | -0.009 m | 0.012 m |

Table B.1: Corresponding points and planes to the curves (from A to J).

| Curves | Planes (y=0 m; z=0 m) | Points | Coordinate y | Coordinate z |
|---|---|---|---|---|
| Curve 12 (O') | Plane 1 | Point 41 | -0.025 m | 0 m |
| | Plane 2 | Point 42 | -0.025 m | 0 m |
| | Plane 3 | Point 43 | -0.025 m | 0 m |
| | Plane 4 | Point 44 | -0.025 m | 0 m |

Table B.2: Corresponding points and planes to the curve 12, which crosses the center of the bell mouth.

| Curves | Planes (y=0 m; z=0 m) | Points | Coordinate y | Coordinate z |
|---|---|---|---|---|
| Curve 13 (K) | Plane 1 | Point 45 | -0.010 m | 0 m |
| | Plane 2 | Point 46 | -0.009 m | 0 m |
| | Plane 3 | Point 47 | -0.010 m | 0 m |
| | Plane 4 | Point 48 | -0.010 m | 0 m |
| Curve 14 (L) | Plane 1 | Point 49 | -0.013 m | -0.009 m |
| | Plane 2 | Point 50 | -0.012 m | -0.009 m |
| | Plane 3 | Point 51 | -0.013 m | -0.009 m |
| | Plane 4 | Point 52 | -0.013 m | -0.009 m |
| Curve 15 (M) | Plane 1 | Point 53 | -0.020 m | -0.014 m2 |
| | Plane 2 | Point 54 | -0.020 m | -0.015 m |
| | Plane 3 | Point 55 | -0.020 m | -0.014 m |
| | Plane 4 | Point 56 | -0.020 m | -0.014 m |
| Curve 16 (N) | Plane 1 | Point 57 | -0.030 m | -0.014 m |
| | Plane 2 | Point 58 | -0.030 m | -0.015 m |
| | Plane 3 | Point 59 | -0.030 m | -0.014 m |
| | Plane 4 | Point 60 | -0.030 m | -0.014 m |
| Curve 17 (O) | Plane 1 | Point 61 | -0.037 m | -0.009 m |
| | Plane 2 | Point 62 | -0.038 m | -0.009 m |
| | Plane 3 | Point 63 | -0.037 m | -0.009 m |
| | Plane 4 | Point 64 | -0.037 m | -0.009 m |
| Curve 18 (P) | Plane 1 | Point 65 | -0.040 m | 0 m |
| | Plane 2 | Point 66 | -0.041 m | 0 m |
| | Plane 3 | Point 67 | -0.040 m | 0 m |
| | Plane 4 | Point 68 | -0.040 m | 0 m |
| Curve 19 (Q) | Plane 1 | Point 69 | -0.037 m | 0.009 m |
| | Plane 2 | Point 70 | -0.038 m | 0.009 m |
| | Plane 3 | Point 71 | -0.037 m | 0.009 m |
| | Plane 4 | Point 72 | -0.037 m | 0.009 m |
| Curve 20 (R) | Plane 1 | Point 73 | -0.030 m | 0.014 m |
| | Plane 2 | Point 74 | -0.030 m | 0.015 m |
| | Plane 3 | Point 75 | -0.030 m | 0.014 m |
| | Plane 4 | Point 76 | -0.030 m | 0.014 m |
| Curve 21 (S) | Plane 1 | Point 77 | -0.020 m | 0.014 m |
| | Plane 2 | Point 78 | -0.020 m | 0.015 m |
| | Plane 3 | Point 79 | -0.020 m | 0.014 m |
| | Plane 4 | Point 80 | -0.020 m | 0.014 m |
| Curve 22 (T) | Plane 1 | Point 81 | -0.013 m | 0.009 m |
| | Plane 2 | Point 82 | -0.012 m | 0.009 m |
| | Plane 3 | Point 83 | -0.013 m | 0.009 m |
| | Plane 4 | Point 84 | -0.013 m | 0.009 m |

Table B.3: Corresponding points and planes to the curves (from K to T).

| Curves | Planes (y=0 m; z=0 m) | Points | Coordinate y | Coordinate z |
|---|---|---|---|---|
| Curve 23 (U) | Plane 1 | Point 85 | -0.015 m | 0 m |
| | Plane 2 | Point 86 | -0.014 m | 0 m |
| | Plane 3 | Point 87 | -0.015 m | 0 m |
| | Plane 4 | Point 88 | -0.015 m | 0 m |
| Curve 24 (V) | Plane 1 | Point 89 | -0.017 m | -0.006 m |
| | Plane 2 | Point 90 | -0.016 m | -0.006 m |
| | Plane 3 | Point 91 | -0.017 m | -0.006 m |
| | Plane 4 | Point 92 | -0.017 m | -0.006 m |
| Curve 25 (W) | Plane 1 | Point 93 | -0.022 m | -0.010 m |
| | Plane 2 | Point 94 | -0.022 m | -0.010 m |
| | Plane 3 | Point 95 | -0.022 m | -0.010 m |
| | Plane 4 | Point 96 | -0.022 m | -0.010 m |
| Curve 26 (X) | Plane 1 | Point 97 | -0.028 m | -0.010 m |
| | Plane 2 | Point 98 | -0.028 m | -0.010 m |
| | Plane 3 | Point 99 | -0.028 m | -0.010 m |
| | Plane 4 | Point 100 | -0.028 m | -0.010 m |
| Curve 27 (Y) | Plane 1 | Point 101 | -0.033 m | -0.006 m |
| | Plane 2 | Point 102 | -0.034 m | -0.006 m |
| | Plane 3 | Point 103 | -0.033 m | -0.006 m |
| | Plane 4 | Point 104 | -0.033 m | -0.006 m |
| Curve 28 (Z) | Plane 1 | Point 105 | -0.035 m | 0 m |
| | Plane 2 | Point 106 | -0.036 m | 0 m |
| | Plane 3 | Point 107 | -0.035 m | 0 m |
| | Plane 4 | Point 108 | -0.035 m | 0 m |
| Curve 29 (A') | Plane 1 | Point 109 | -0.033 m | 0.006 m |
| | Plane 2 | Point 110 | -0.034 m | 0.006 m |
| | Plane 3 | Point 111 | -0.033 m | 0.006 m |
| | Plane 4 | Point 112 | -0.033 m | 0.006 m |
| Curve 30 (B') | Plane 1 | Point 113 | -0.028 m | 0.010 m |
| | Plane 2 | Point 114 | -0.028 m | 0.010 m |
| | Plane 3 | Point 115 | -0.028 m | 0.010 m |
| | Plane 4 | Point 116 | -0.028 m | 0.010 m |
| Curve 31 (C') | Plane 1 | Point 117 | -0.022 m | 0.010 m |
| | Plane 2 | Point 118 | -0.022 m | 0.010 m |
| | Plane 3 | Point 119 | -0.022 m | 0.010 m |
| | Plane 4 | Point 120 | -0.022 m | 0.010 m |
| Curve 32 (D') | Plane 1 | Point 121 | -0.017 m | 0.006 m |
| | Plane 2 | Point 122 | -0.016 m | 0.006 m |
| | Plane 3 | Point 123 | -0.017 m | 0.006 m |
| | Plane 4 | Point 124 | -0.017 m | 0.006 m |

Table B.4: Corresponding points and planes to the curves (from U to D').

| Curves | Planes (y=0 m; z=0 m) | Points | Coordinate y | Coordinate z |
|---|---|---|---|---|
| Curve 33 (E') | Plane 1 | Point 125 | -0.020 m | 0 m |
| | Plane 2 | Point 126 | -0.019 m | 0 m |
| | Plane 3 | Point 127 | -0.020 m | 0 m |
| | Plane 4 | Point 128 | -0.020 m | 0 m |
| Curve 34 (F') | Plane 1 | Point 129 | -0.021 m | -0.003 m |
| | Plane 2 | Point 130 | -0.020 m | -0.003 m |
| | Plane 3 | Point 131 | -0.021 m | -0.003 m |
| | Plane 4 | Point 132 | -0.021 m | -0.003 m |
| Curve 35 (G') | Plane 1 | Point 133 | -0.023 m | -0.005 m |
| | Plane 2 | Point 134 | -0.023 m | -0.005 m |
| | Plane 3 | Point 135 | -0.023 m | -0.005 m |
| | Plane 4 | Point 136 | -0.023 m | -0.005 m |
| Curve 36 (H') | Plane 1 | Point 137 | -0.027 m | -0.005 m |
| | Plane 2 | Point 138 | -0.027 m | -0.005 m |
| | Plane 3 | Point 139 | -0.027 m | -0.005 m |
| | Plane 4 | Point 140 | -0.027 m | -0.005 m |
| Curve 37 (I') | Plane 1 | Point 141 | -0.029 m | -0.003 m |
| | Plane 2 | Point 142 | -0.030 m | -0.003 m |
| | Plane 3 | Point 143 | -0.029 m | -0.003 m |
| | Plane 4 | Point 144 | -0.029 m | -0.003 m |
| Curve 38 (J') | Plane 1 | Point 145 | -0.030 m | 0 m |
| | Plane 2 | Point 146 | -0.031 m | 0 m |
| | Plane 3 | Point 147 | -0.030 m | 0 m |
| | Plane 4 | Point 148 | -0.030 m | 0 m |
| Curve 39 (K') | Plane 1 | Point 149 | -0.029 m | 0.003 m |
| | Plane 2 | Point 150 | -0.030 m | 0.003 m |
| | Plane 3 | Point 151 | -0.029 m | 0.003 m |
| | Plane 4 | Point 152 | -0.029 m | 0.003 m |
| Curve 40 (L') | Plane 1 | Point 153 | -0.027 m | 0.005 m |
| | Plane 2 | Point 154 | -0.027 m | 0.005 m |
| | Plane 3 | Point 155 | -0.027 m | 0.005 m |
| | Plane 4 | Point 156 | -0.027 m | 0.005 m |
| Curve 41 (M') | Plane 1 | Point 157 | -0.023 m | 0.005 m |
| | Plane 2 | Point 158 | -0.023 m | 0.005 m |
| | Plane 3 | Point 159 | -0.023 m | 0.005 m |
| | Plane 4 | Point 160 | -0.023 m | 0.005 m |
| Curve 42 (N') | Plane 1 | Point 161 | -0.021 m | 0.003 m |
| | Plane 2 | Point 162 | -0.020 m | 0.003 m |
| | Plane 3 | Point 163 | -0.021 m | 0.003 m |
| | Plane 4 | Point 164 | -0.021 m | 0.003 m |

Table B.5: Corresponding points and planes to the curves (from E' to N').

# APPENDIX C. RESULTS OF VELOCITY, STATIC PRESSURE, AND TOTAL PRESSURE FOR POINTS CONTAINED ON CROSS-SECTIONAL PLANES 1 TO 3 (AT AN OUTLET STATIC PRESSURE OF 100075 PA)

| Curves | Planes (x=value) | Total pressure | Static pressure | Velocity |
|---|---|---|---|---|
| Curve 2 (A) | -0.035 m | 101259.27 Pa | 100113.82 Pa | 43.34 m/s |
| | -0.030 m | 101245.11 Pa | 100073.41 | 43.84 m/s |
| | -0.020 m | 101242.52 Pa | 100083.29 Pa | 43.61 m/s |
| Curve 3 (B) | -0.035 m | 101265.18 Pa | 100111.58 Pa | 43.49 m/s |
| | -0.030 m | 101256.02 Pa | 100071.50 Pa | 44.07 m/s |
| | -0.020 m | 101249.49 Pa | 1100081.23 Pa | 43.78 m/s |
| Curve 4 (C) | -0.035 m | 101162.55 Pa | 100018.007 Pa | 43.34 m/s |
| | -0.030 m | 101247.32 Pa | 100070.99 Pa | 43.95 m/s |
| | -0.020 m | 101243.13 Pa | 100082.67 Pa | 43.63 m/s |
| Curve 5 (D) | -0.035 m | 101258.81 Pa | 100109.23 Pa | 43.41 m/s |
| | -0.030 m | 101248.05 Pa | 100070.69 Pa | 43.97 m/s |
| | -0.020 m | 101243.74 Pa | 100082.61 Pa | 43.648 m/s |
| Curve 6 (E) | -0.035 m | 101265.10 Pa | 100111.18 Pa | 43.49 m/s |
| | -0.030 m | 101256.11 Pa | 100071.26 Pa | 44.085 m/s |
| | -0.020 m | 101249.37 Pa | 100081.32 Pa | 43.77 m/s |
| Curve 7 (F) | -0.035 m | 101259.10 Pa | 100113.47 Pa | 43.34 m/s |
| | -0.030 m | 101245.09 Pa | 100073.12 Pa | 43.84 m/s |
| | -0.020 m | 101242.15 Pa | 100083.17 Pa | 43.607 m/s |
| Curve 8 (G) | -0.035 m | 101265.63 Pa | 100110.88 Pa | 43.51 m/s |
| | -0.030 m | 101255.50 Pa | 100071.58 | 44.069 m/s |
| | -0.020 m | 101249.17 Pa | 100080.85 Pa | 43.781 m/s |
| Curve 9 (H) | -0.035 m | 101258.89 Pa | 1100109.02 Pa | 43.420 m/s |
| | -0.030 m | 101247.54 Pa | 100070.97 Pa | 43.967 m/s |
| | -0.020 m | 101243.35 Pa | 100082.34 Pa | 43.645 m/s |
| Curve 10 (I) | -0.035 m | 101258.55 Pa | 100109.29 Pa | 43.408 m/s |
| | -0.030 m | 101247.16 Pa | 100071.30 Pa | 43.95 m/s |
| | -0.020 m | 101243.19 Pa | 100082.62 Pa | 43.637 m/s |
| Curve 11 (J) | -0.035 m | 101265.37 Pa | 100111.11 Pa | 43.503 m/s |
| | -0.030 m | 101255.48 Pa | 100072.07 Pa | 44.059 m/s |
| | -0.020 m | 101249.65 Pa | 100081.08 Pa | 43.786 m/s |

Table C.1: Values of velocity and pressure of the points corresponding to the curves from A to J.

| Curves | Planes (x=value) | Total pressure | Static pressure | Velocity |
|---|---|---|---|---|
| Curve 12 (O') | -0.035 m | 101303.09 Pa | 100258.44 Pa | 41.345 m/s |
| | -0.030 m | 101293.06 Pa | 100149.42 | 43.300 m/s |
| | -0.020 m | 101289.93 Pa | 100111.11 Pa | 43.968 m/s |

Table C.2: Values of velocity and pressure of the points corresponding to the curve that crosses the center line of the bell mouth (curve O').

| Curves | Planes (x=value) | Total pressure | Static pressure | Velocity |
|---|---|---|---|---|
| Curve 13 (K) | -0.035 m | 101274.39 Pa | 100168.17 Pa | 42.57 m/s |
| | -0.030 m | 101268.39 Pa | 100118.54 Pa | 43.424 m/s |
| | -0.020 m | 101266.50 Pa | 100091.589 Pa | 43.902 m/s |
| Curve 14 (L) | -0.035 m | 101279.49 Pa | 100189.90 Pa | 42.250 m/s |
| | -0.030 m | 101271.08 Pa | 100114.33 Pa | 43.553 m/s |
| | -0.020 m | 101268.48 Pa | 100088.86 Pa | 43.99 m/s |
| Curve 15 (M) | -0.035 m | 101278.64 Pa | 100193.75 Pa | 42.14 m/s |
| | -0.030 m | 101270.76 Pa | 100136.030 Pa | 43.144 m/s |
| | -0.020 m | 101267.34 Pa | 100090.29 Pa | 43.942 m/s |
| Curve 16 (N) | -0.035 m | 101278.74 Pa | 100193.623 Pa | 42.147 m/s |
| | -0.030 m | 101271.61 Pa | 100133.887 Pa | 43.19 m/s |
| | -0.020 m | 101266.73 Pa | 1100090.18 Pa | 43.93 m/s |
| Curve 17 (O) | -0.035 m | 101280.19 Pa | 100189.68 Pa | 42.25 m/s |
| | -0.030 m | 101273.60 Pa | 100128.73 Pa | 43.32 m/s |
| | -0.020 m | 101267.34 Pa | 100088.53 Pa | 43.97 m/s |
| Curve 18 (P) | -0.035 m | 101274.24 Pa | 100194.64 Pa | 42.11 m/s |
| | -0.030 m | 101270.26 Pa | 100133.39 Pa | 43.424 m/s |
| | -0.020 m | 101266.28 Pa | 100091.63 Pa | 43.897 m/s |
| Curve 19 (Q) | -0.035 m | 101279.70 Pa | 100189.86 Pa | 42.255 m/s |
| | -0.030 m | 101273.51 Pa | 100128.88 Pa | 43.32 m/s |
| | -0.020 m | 101267.83 Pa | 100088.67 Pa | 43.98 m/s |
| Curve 20 (R) | -0.035 m | 101278.78 Pa | 100193.70 Pa | 42.145 m/s |
| | -0.030 m | 101269.99 Pa | 100134.089 Pa | 43.452 m/s |
| | -0.020 m | 101267.49 Pa | 1100090.325 Pa | 43.94 m/s |
| Curve 21 (S) | -0.035 m | 101278.34 Pa | 100193.87 Pa | 42.144 m/s |
| | -0.030 m | 101271.64 Pa | 100134.30 Pa | 43.445 m/s |
| | -0.020 m | 101266.98 Pa | 100090.282 Pa | 43.936 m/s |
| Curve 22 (T) | -0.035 m | 101280.11 Pa | 100190.22 Pa | 42.245 m/s |
| | -0.030 m | 101273.37 Pa | 100129.55 | 43.306 m/s |
| | -0.020 m | 101267.94 Pa | 100088.81 Pa | 43.981 m/s |

Table C.3: Values of velocity and pressure of the points corresponding to the curves from K to T.

| Curves | Planes (x=value) | Total pressure | Static pressure | Velocity |
|---|---|---|---|---|
| Curve 23 (U) | -0.035 m | 101288.68 Pa | 100234.74 Pa | 41.54 m/s |
| | -0.030 m | 101283.42 Pa | 100166.78 Pa | 42.78 m/s |
| | -0.020 m | 101278.66 Pa | 100099.69 Pa | 43.976 m/s |
| Curve 24 (V) | -0.035 m | 101289.73 Pa | 100228.644 Pa | 41.666 m/s |
| | -0.030 m | 101284.02 Pa | 100167.57 Pa | 42.778 m/s |
| | -0.020 m | 101278.270 Pa | 100097.973 Pa | 44.00 m/s |
| Curve 25 (W) | -0.035 m | 101289.18 Pa | 100233.22 Pa | 41.58 m/s |
| | -0.030 m | 101284.05 Pa | 100169.02 Pa | 42.79 m/s |
| | -0.020 m | 101278.95 Pa | 100098.86 Pa | 43.99 m/s |
| Curve 26 (X) | -0.035 m | 101288.92 Pa | 100233.18 Pa | 41.58 m/s |
| | -0.030 m | 101283.77 Pa | 100166.84 Pa | 42.79 m/s |
| | -0.020 m | 101278.55 Pa | 100098.94 Pa | 43.98 m/s |
| Curve 27 (Y) | -0.035 m | 101289.47 Pa | 100228.59 Pa | 41.66 m/s |
| | -0.030 m | 101283.74 Pa | 100167.48 Pa | 42.77 m/s |
| | -0.020 m | 101277.63 Pa | 100097.94 Pa | 43.98 m/s |
| Curve 28 (Z) | -0.035 m | 101288.30 Pa | 100234.70 Pa | 41.54 m/s |
| | -0.030 m | 101282.86 Pa | 100166.82 Pa | 42.77 m/s |
| | -0.020 m | 101278.84 Pa | 100100.06 Pa | 43.97 m/s |
| Curve 29 (A') | -0.035 m | 101289.69 Pa | 100228.62 Pa | 41.66 m/s |
| | -0.030 m | 101284.14 Pa | 100167.41 Pa | 42.78 m/s |
| | -0.020 m | 101278.00 Pa | 100097.88 Pa | 43.99 m/s |
| Curve 30 (B') | -0.035 m | 101288.96 Pa | 100233.15 Pa | 41.583 m/s |
| | -0.030 m | 101283.92 Pa | 100166.86 Pa | 42.79 m/s |
| | -0.020 m | 101278.88 Pa | 100098.88 Pa | 43.995 m/s |
| Curve 31 (C') | -0.035 m | 101289.16 Pa | 100233.16 Pa | 41.58 m/s |
| | -0.030 m | 101284.36 Pa | 100166.82 Pa | 42.80 m/s |
| | -0.020 m | 101278.55 Pa | 100098.70 Pa | 43.992 m/s |
| Curve 32 (D') | -0.035 m | 101288.80 Pa | 100228.71 Pa | 41.66 m/s |
| | -0.030 m | 101284.13 Pa | 100167.72 | 42.77 m/s |
| | -0.020 m | 101277.88 Pa | 100097.75 Pa | 43.99 m/s |

Table C.4: Values of velocity and pressure of the points corresponding to the curves from U' to D'.

| Curves | Planes (x=value) | Total pressure | Static pressure | Velocity |
|---|---|---|---|---|
| Curve 33 (E') | -0.035 m | 101295.99 Pa | 100247.02 Pa | 41.43 m/s |
| | -0.030 m | 101291.29 Pa | 100193.44 Pa | 42.39 m/s |
| | -0.020 m | 101284.69 Pa | 100106.93 Pa | 43.95 m/s |
| Curve 34 (F') | -0.035 m | 101294.12 Pa | 100241.58 Pa | 41.50 m/s |
| | -0.030 m | 101287.25 Pa | 100161.48 Pa | 42.94 m/s |
| | -0.020 m | 101283.13 Pa | 100104.86 Pa | 43.96 m/s |
| Curve 35 (G') | -0.035 m | 101294.66 Pa | 100243.522 Pa | 41.47 m/s |
| | -0.030 m | 101290.27 Pa | 100190.47 Pa | 42.43 m/s |
| | -0.020 m | 101283.67 Pa | 100105.66 Pa | 43.955 m/s |
| Curve 36 (H') | -0.035 m | 101294.64 Pa | 100243.48 Pa | 41.47 m/s |
| | -0.030 m | 101290.20 Pa | 100190.44 Pa | 42.43 m/s |
| | -0.020 m | 101283.56 Pa | 100105.65 Pa | 43.953 m/s |
| Curve 37 (I') | -0.035 m | 101294.04 Pa | 100241.549 Pa | 41.499 m/s |
| | -0.030 m | 101289.69 Pa | 100188.76 Pa | 42.458 m/s |
| | -0.020 m | 101282.997 Pa | 100104.91 Pa | 43.956 m/s |
| Curve 38 (J') | -0.035 m | 101295.799 Pa | 100247.016 Pa | 41.429 m/s |
| | -0.030 m | 101291.078 Pa | 100193.478 Pa | 42.393 m/s |
| | -0.020 m | 101284.764 Pa | 100107.086 Pa | 43.948 m/s |
| Curve 39 (K') | -0.035 m | 101294.053 Pa | 100241.566 Pa | 41.499 m/s |
| | -0.030 m | 101287.27 Pa | 100188.75 Pa | 42.46 m/s |
| | -0.020 m | 101283.082 Pa | 100104.91 Pa | 43.958 m/s |
| Curve 40 (L') | -0.035 m | 101294.67 Pa | 100243.46 Pa | 41.475 m/s |
| | -0.030 m | 101290.29 Pa | 100190.39 Pa | 42.438 m/s |
| | -0.020 m | 101283.61 Pa | 100105.64 Pa | 43.954 m/s |
| Curve 41 (M') | -0.035 m | 101294.70 Pa | 100243.51 Pa | 41.474 m/s |
| | -0.030 m | 101290.34 Pa | 100190.43 Pa | 42.438 m/s |
| | -0.020 m | 101283.62 Pa | 100105.63 Pa | 43.954 m/s |
| Curve 42 (N') | -0.035 m | 101294.16 Pa | 100241.61 Pa | 41.500 m/s |
| | -0.030 m | 1101289.89 Pa | 100188.78 | 42.461 m/s |
| | -0.020 m | 101283.05 Pa | 100104.84 Pa | 43.959 m/s |

Table C.5: Values of velocity and pressure of the points corresponding to the curves from E' to N'.

# APPENDIX D. PRESSURE AND VELOCITY PROFILES

## D.0.1.. Total-Pressure profiles

### *D.0.1.1.. Cross-section 1 (x=-0.020 m). Results of radial lines 1 to 8*


Figure D.1: Total-pressure profile for radial lines 1 to 8 (different angles) at an outlet static pressure 99500 Pa.

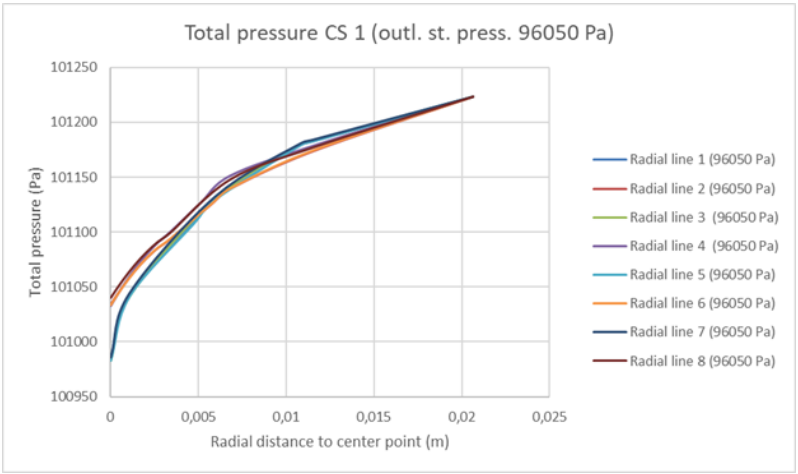


Figure D.2: Total-pressure profile for radial lines 1 to 8 (different angles) at an outlet static pressure 96050 Pa.

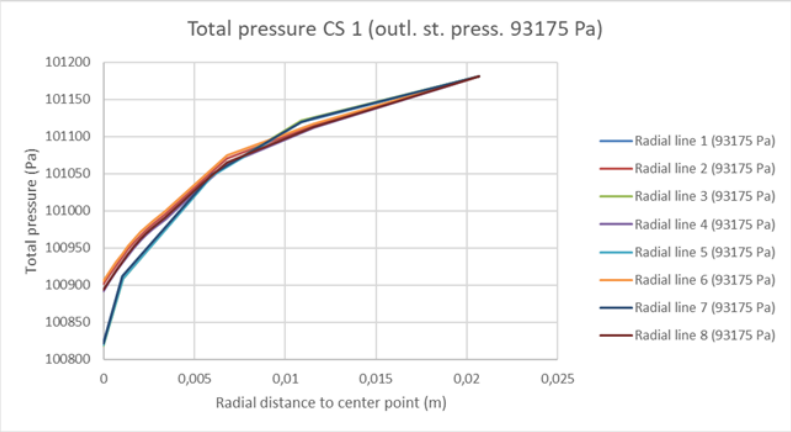


Figure D.3: Total-pressure profile for radial lines 1 to 8 (different angles) at an outlet static pressure 93175 Pa.

*D.0.1.2.. Cross-section 2 (x=-0.030 m). Results of radial lines 1' to 8'*

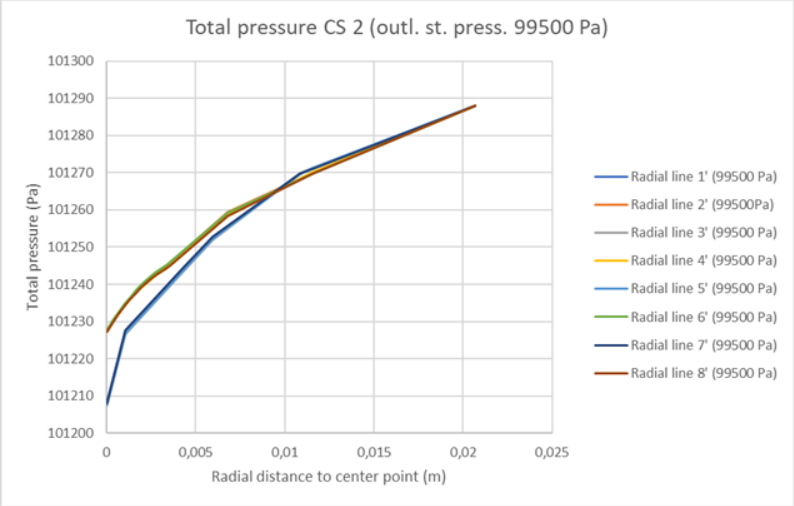


Figure D.4: Total-pressure profile for radial lines 1' to 8' (different angles) at an outlet static pressure 99500 Pa.

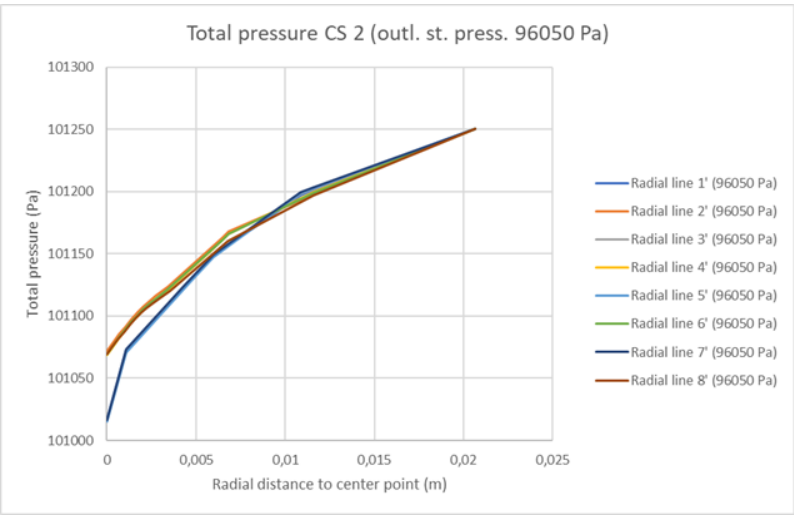


Figure D.5: Total-pressure profile for radial lines 1' to 8' (different angles) at an outlet static pressure 96050 Pa

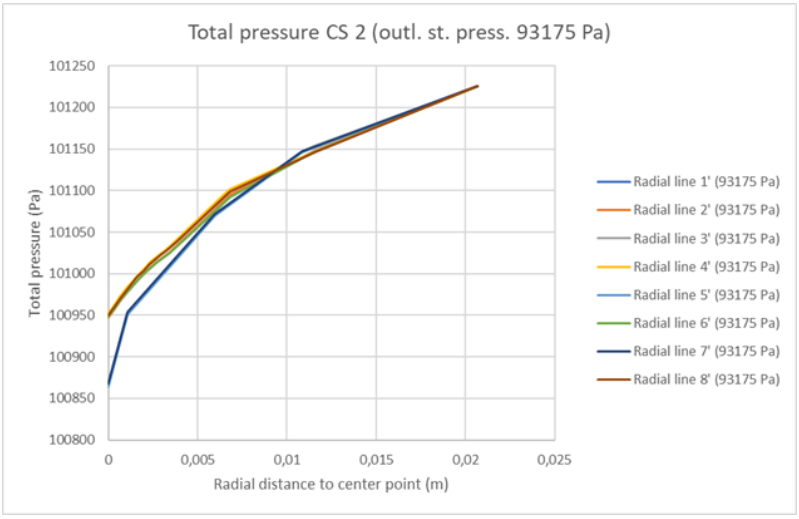


Figure D.6: Total-pressure profile for radial lines 1’ to 8’ (different angles) at an outlet static pressure 93175 Pa.

*D.0.1.3.. Cross-section 3 (x=-0.035 m). Results of radial lines 1" to 8"*

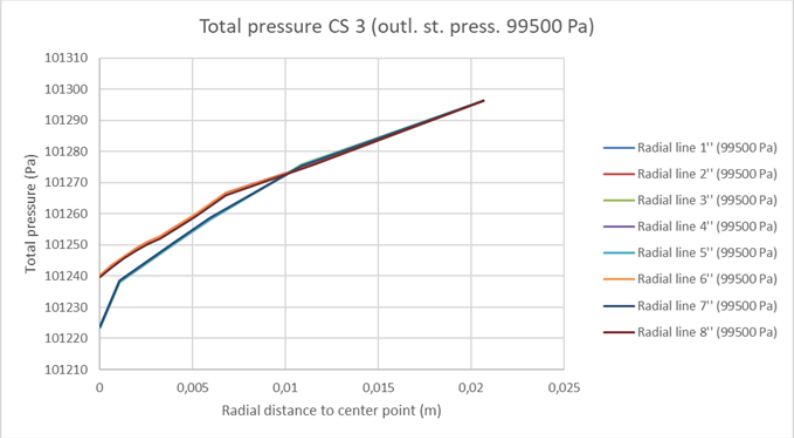


Figure D.7: Total-pressure profile for radial lines 1" to 8" (different angles) at an outlet static pressure 99500 Pa.

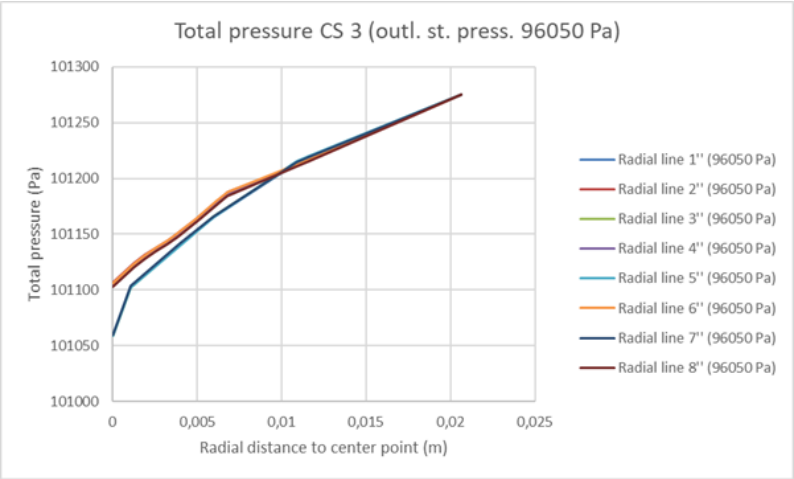


Figure D.8: Total-pressure profile for radial lines 1" to 8" (different angles) at an outlet static pressure 96050 Pa.

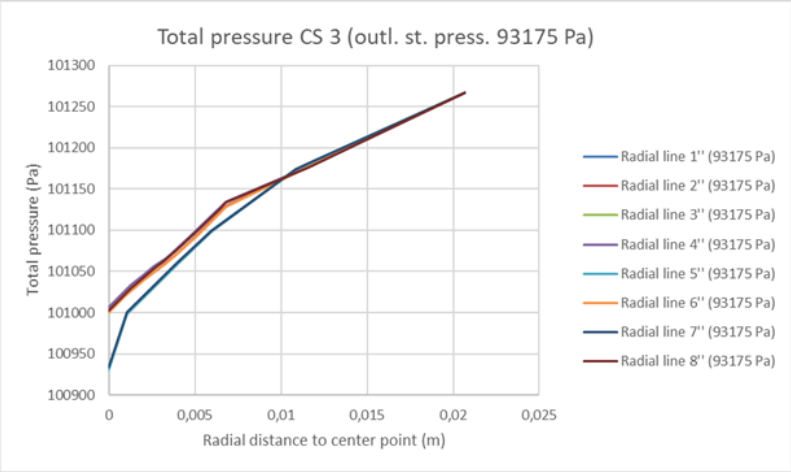


Figure D.9: Total-pressure profile for radial lines 1” to 8” (different angles) at an outlet static pressure 93175 Pa.

## D.0.2.. Static-pressure profiles

### *D.0.2.1.. Cross-section 1 (x=-0.020 m). Results of radial lines 1 to 8*

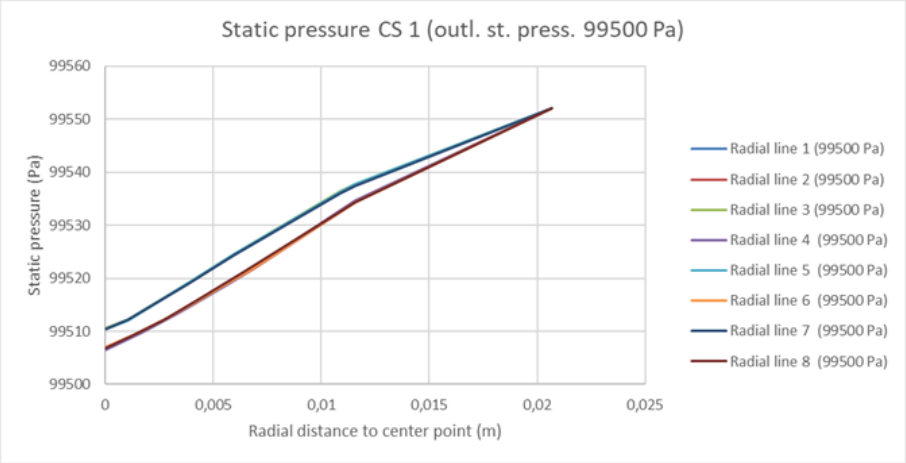


Figure D.10: Static-pressure profile for radial lines 1 to 8 (different angles) at an outlet static pressure 99500 Pa.

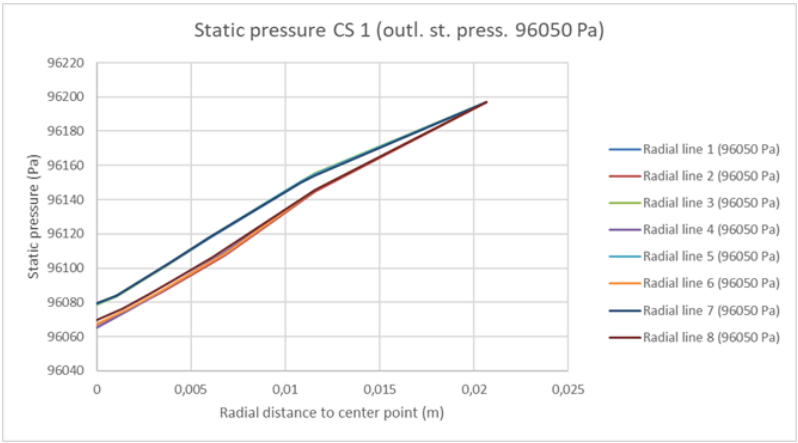


Figure D.11: Static-pressure profile for radial lines 1 to 8 (different angles) at an outlet static pressure 96050 Pa.

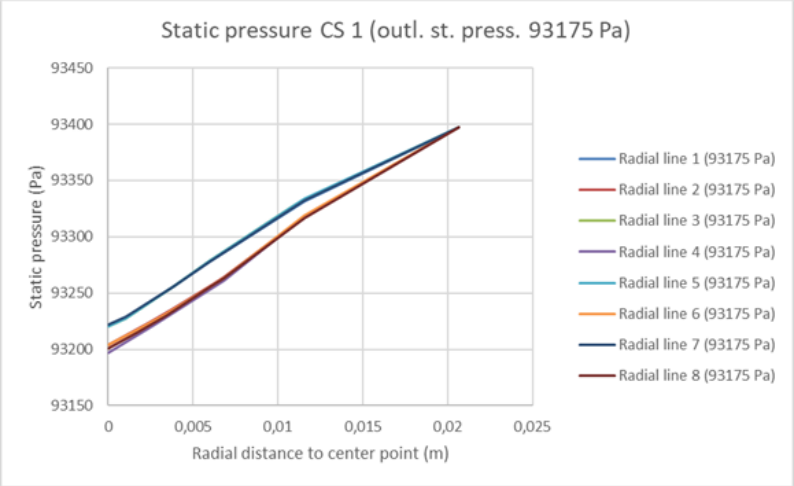


Figure D.12: Static-pressure profile for radial lines 1 to 8 (different angles) at an outlet static pressure 93175 Pa.

*D.0.2.2.. Cross-section 2 (x=-0.030 m). Results of radial lines 1' to 8'*

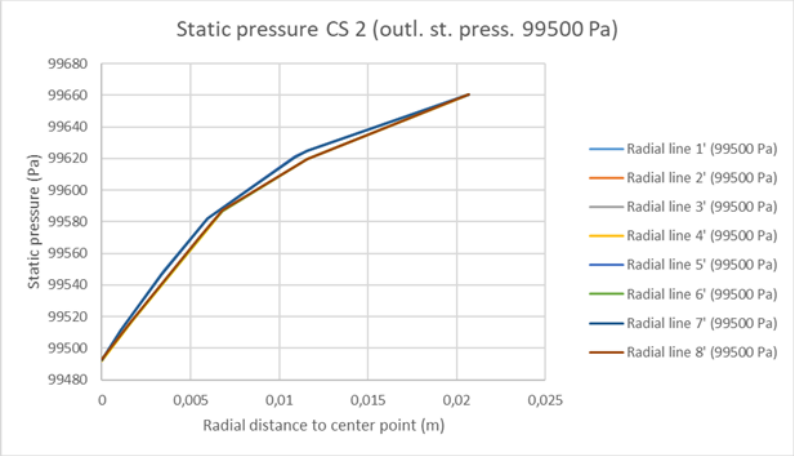


Figure D.13: Static-pressure profile for radial lines 1' to 8' (different angles) at an outlet static pressure 100075 Pa.

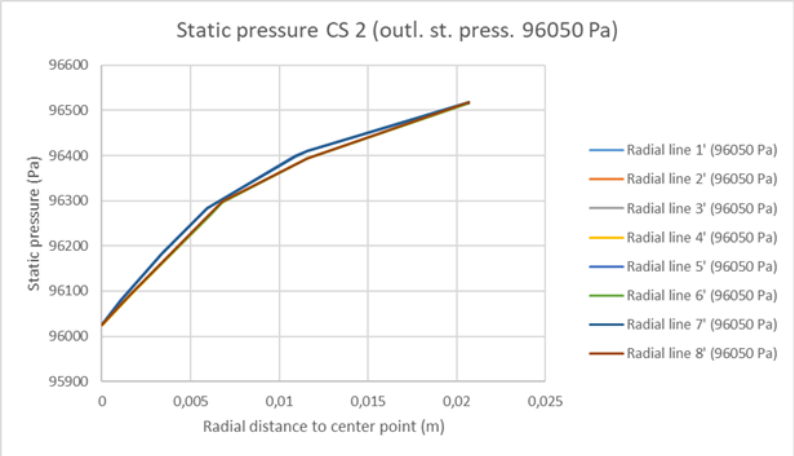


Figure D.14: Static-pressure profile for radial lines 1' to 8' (different angles) at an outlet static pressure 100075 Pa.

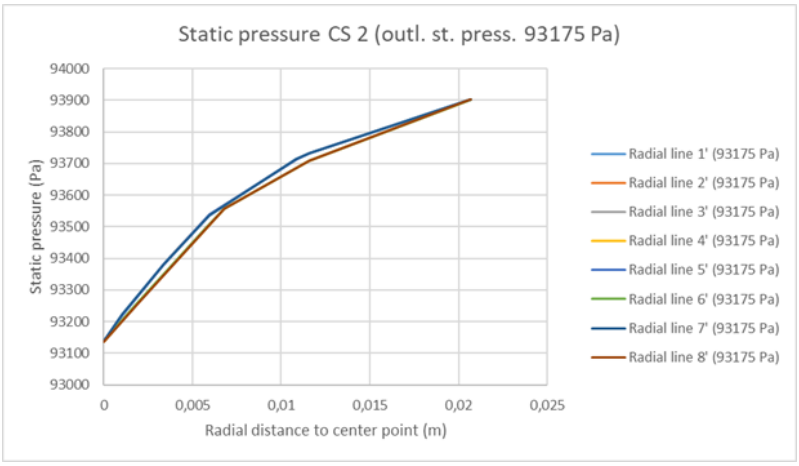


Figure D.15: Static-pressure profile for radial lines 1’ to 8’ (different angles) at an outlet static pressure 100075 Pa.

*D.0.2.3.. Cross-section 3 (x=-0.035 m). Results of radial lines 1” to 8”*

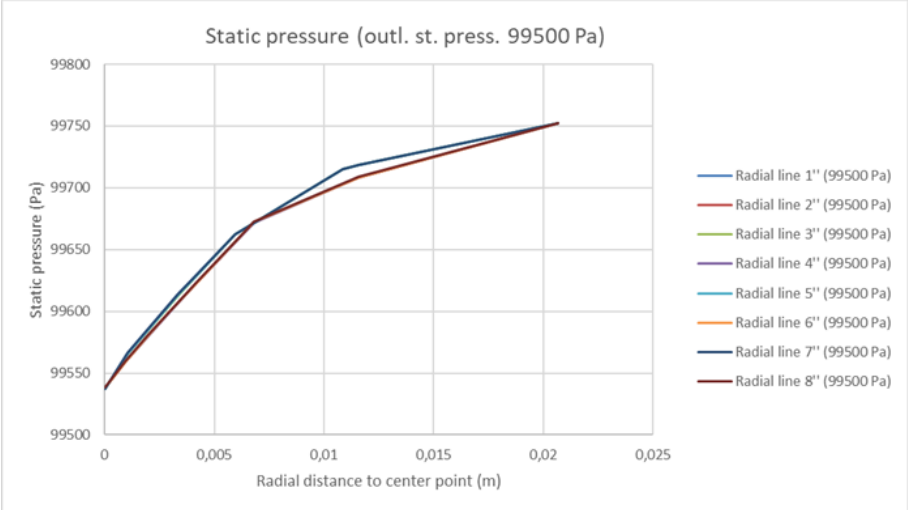


Figure D.16: Static-pressure profile for radial lines 1” to 8” (different angles) at an outlet static pressure 99500 Pa.

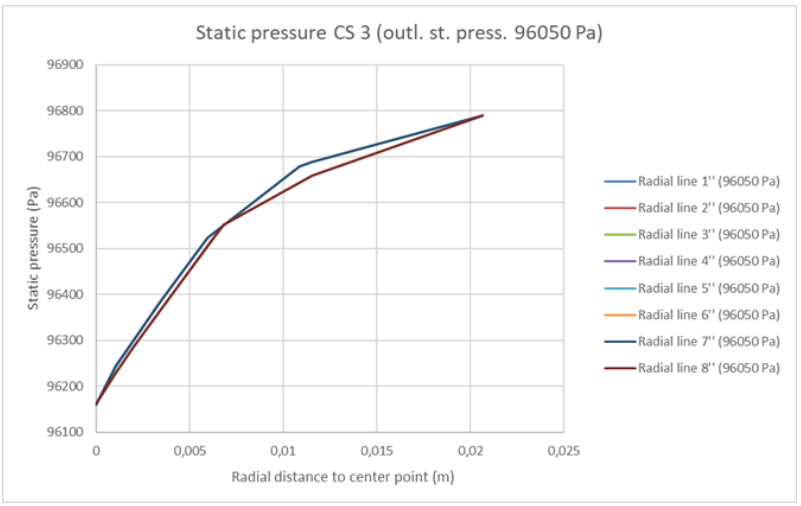


Figure D.17: Static-pressure profile for radial lines 1” to 8” (different angles) at an outlet static pressure 96050 Pa.

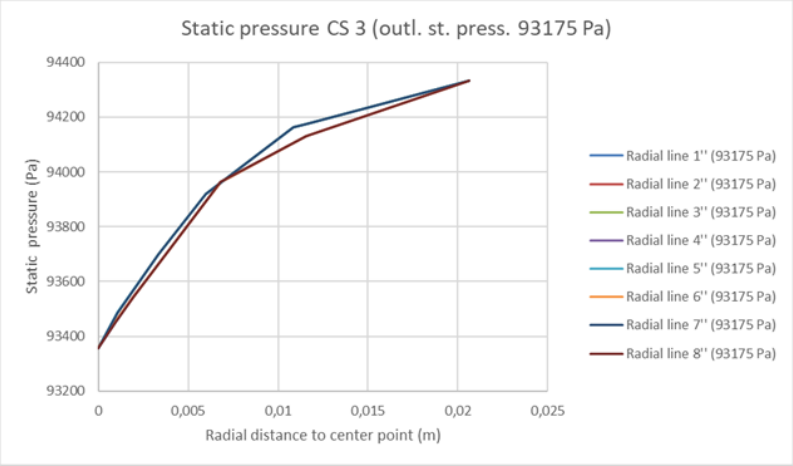


Figure D.18: Static-pressure profile for radial lines 1” to 8” (different angles) at an outlet static pressure 93175 Pa.

## D.0.3.. Velocity profiles

### *D.0.3.1.. Cross-section 1 (x=-0.020 m). Results of radial lines 1 to 8*

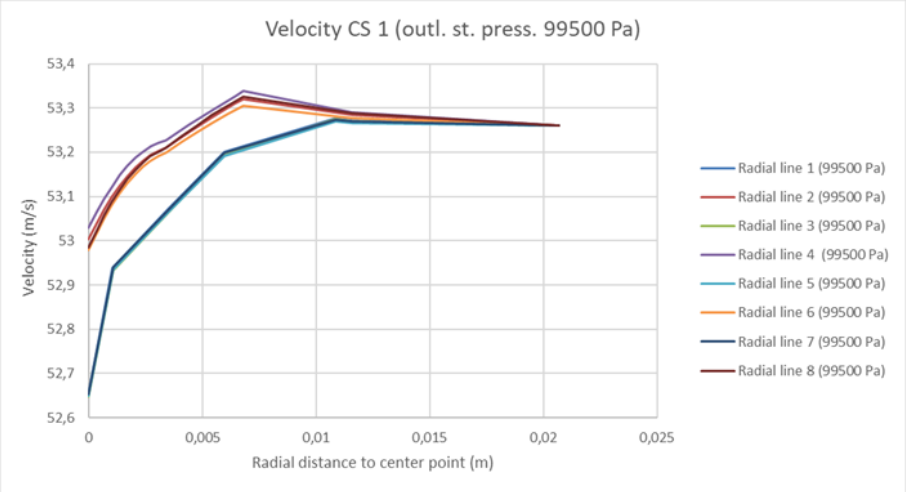


Figure D.19: Velocity profile for radial lines 1 to 8 (different angles) at an outlet static pressure 99500 Pa.

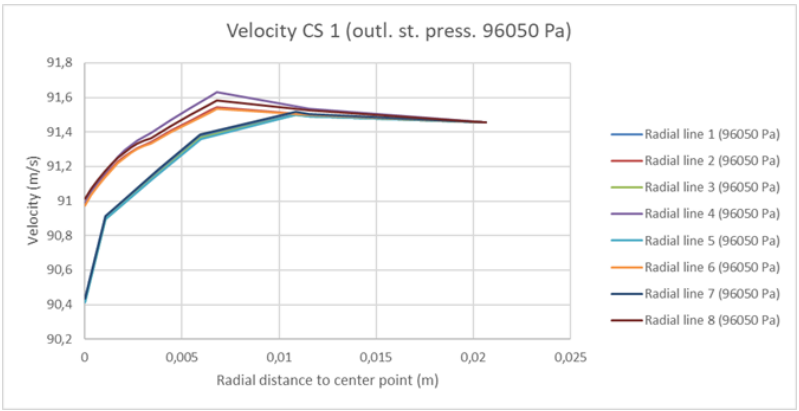


Figure D.20: Velocity profile for radial lines 1 to 8 (different angles) at an outlet static pressure 96050 Pa.

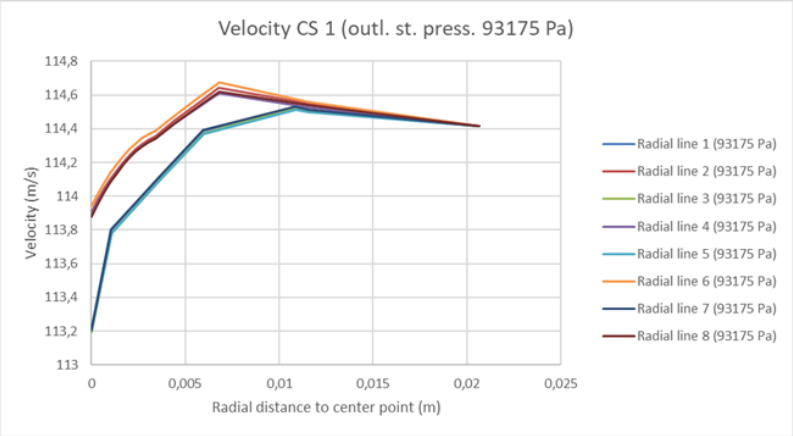


Figure D.21: Velocity profile for radial lines 1 to 8 (different angles) at an outlet static pressure 93175 Pa.

*D.0.3.2.. Cross-section 2 (x=-0.030 m). Results of radial lines 1' to 8'*

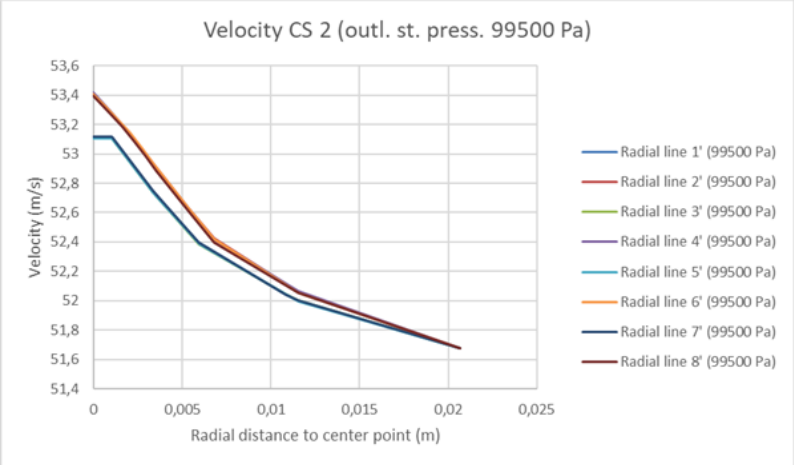


Figure D.22: Velocity profile for radial lines 1' to 8' (different angles) at an outlet static pressure 99500 Pa.

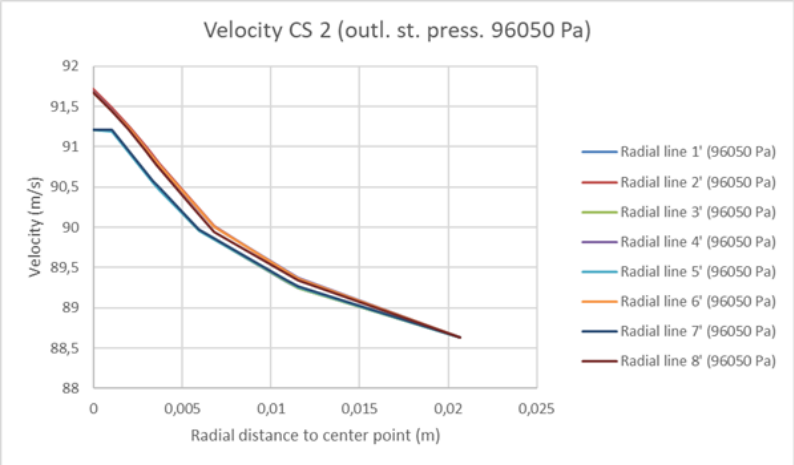


Figure D.23: Velocity profile for radial lines 1' to 8' (different angles) at an outlet static pressure 96050 Pa

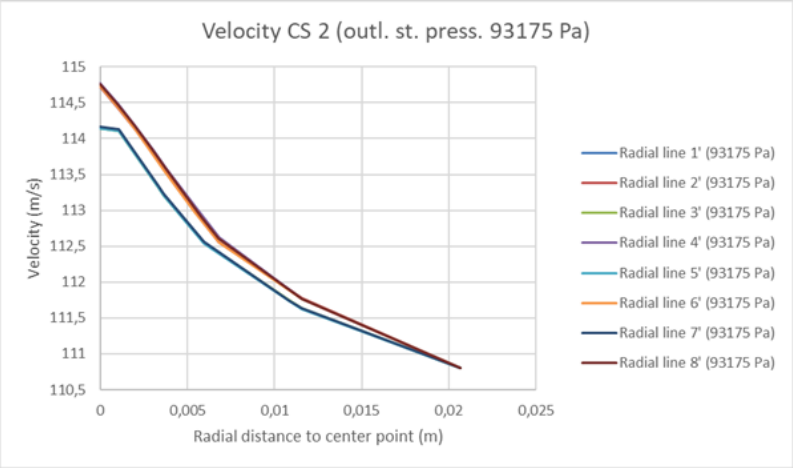


Figure D.24: Velocity profile for radial lines 1' to 8' (different angles) at an outlet static pressure 93175 Pa.

*D.0.3.3.. Cross-section 3 (x=-0.035 m). Results of radial lines 1" to 8"*

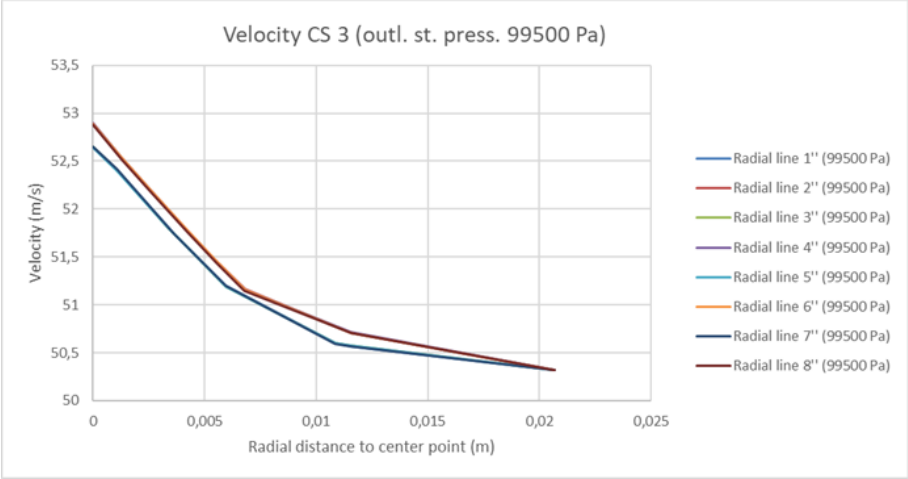


Figure D.25: Velocity profile for radial lines 1" to 8" (different angles) at an outlet static pressure 99500 Pa.

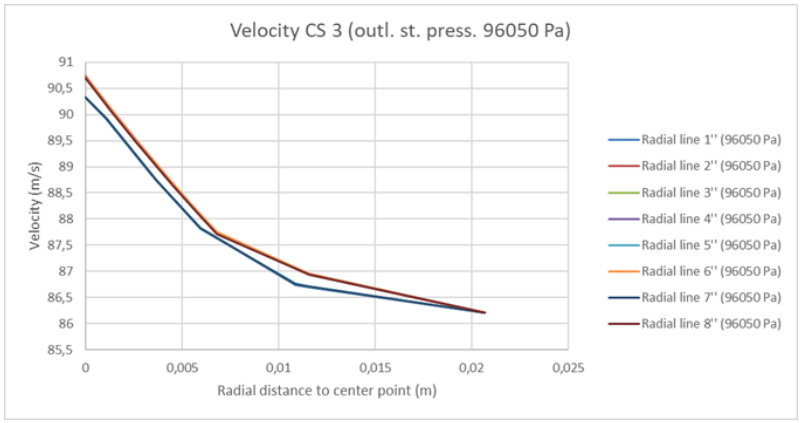


Figure D.26: Velocity profile for radial lines 1" to 8" (different angles) at an outlet static pressure 96050 Pa.

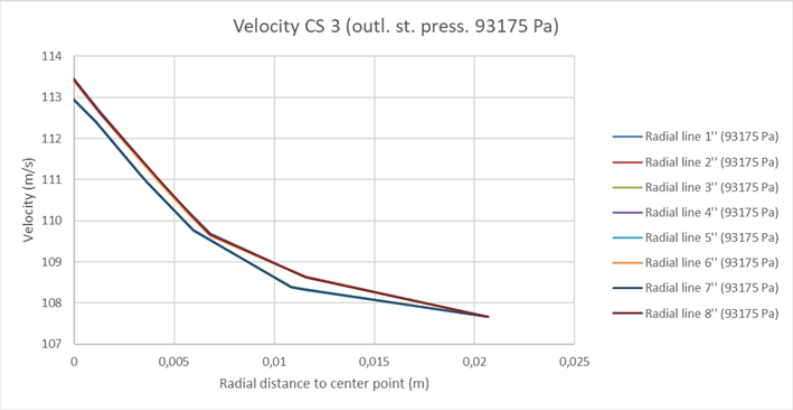


Figure D.27: Velocity profile for radial lines 1” to 8” (different angles) at an outlet static pressure 93175 Pa.

# APPENDIX E. DEVICES' SPECIFICATIONS

## E.1.. Absolute and Gauge Pressure Transducers - Series 2000


Figure E.1: Series 2000 Absolute Pressure Transducer [11]


Figure E.2: Series 2000 Gauge Pressure Transducer [11]

Repeatability : Better than $\pm$ 0.005% Full Scale
Hysteresis : Better than $\pm$ 0.005% Full Scale
Acceleration Sensitivity : $\pm$ 0.0038% Full Scale /g

**Characteristics**

Pressure signal is a frequency output with a 10% frequency change within the frequency band 30 KHz to 42 KHz.

Standard resolution: $\pm$ 0.0001 %FS (6 digits, $\pm$ 0.001 hPa).

maximum drift per year: $<\pm$ 0.10 hPa.

Temperature signal is a frequency output with a 45 ppm/ $^{\circ}$C sensitivity within the band 168 KHz to 176 KHz.

Both pressure and temperature output signals are nominally square waves of 4 volts amplitude peak to peak.

Conformance and temperature compensation equations and calibration coefficients are provided with each transducer.

Weight $\rightarrow$ 15.4 ounces (436 grams) Max
Power Requirements $\rightarrow$ +5 to 16V DC at 1.3 mA Max

**Environmental**

Overpressure $\rightarrow$ 1.2 times Full Scale
Model 2500A-101 $\rightarrow$ 1.0 times Full Scale
Operating Temperature Range $\rightarrow$ -54 $^{\circ}$C to +107 $^{\circ}$C (-65 $^{\circ}$F to 225 $^{\circ}$F)

| Absolute pressure ranges | Model No | Part number |
|---|---|---|
| 0-0.10 MPa | 215A-10X | 1200-00X |
| 0.08-0.11 MPa | 216B-10X | 1141-00X |
| 0-0.16 MPa | 223A-10X | 1201-00X |
| 0-0.21 MPa | 230A-10X | 1202-00X |
| 0-0.31 MPa | 245A-10X | 1203-00X |
| 0-0.69 MPa | 2100A-10X | 1204-00X |
| 0-1.38 MPa | 2200A-10X | 1205-00X |
| 0-2.07 MPa | 2300A-10X | 1206-00X |
| 0-2.76 MPa | 2400A-10X | 1207-00X |
| 0-3.45 MPa | 2500A-101 | 1208-001 |

Table E.1: Absolute pressure ranges [11]

| Gauge pressure ranges | Model No | Part number |
|---|---|---|
| 0-0.01 MPa | 202BG-102 | 1546-002 |
| 0-0.10 MPa | 215G-10X | 1210-00X |
| 0-0.15 MPa | 222G-10X | 1215-00X |
| 0-0.21 MPa | 230G-10X | 1211-00X |
| 0-0.69 MPa | 2100G-10X | 1212-00X |
| 0-1.03 MPa | 2150G-10X( | 1214-00X |
| 0-1.38 MPa | 2200G-10X | 1213-00X |

Table E.2: Gauge pressure ranges [11]

## E.2.. Model 735 Intelligent Display

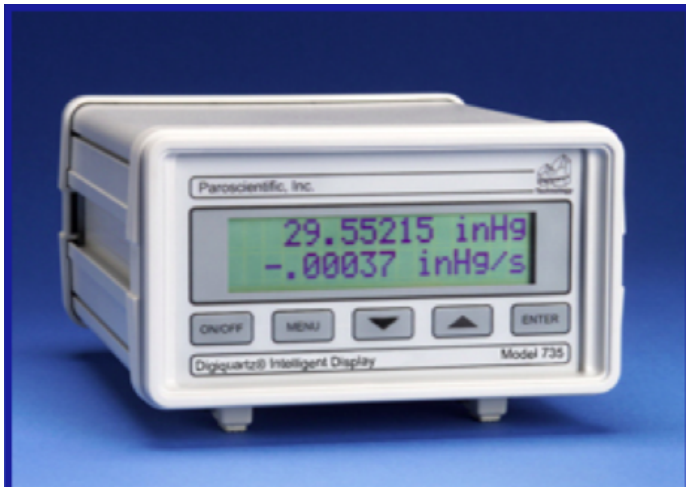


Figure E.3: Model 735 Intelligent Display [26]

The Model 735 Intelligent Display performs all of the functions of the Model 745 High Accuracy Portable Standard with the frequency inputs from one external Digiquartz® Transducer. It contains an intuitive Front Panel Menu System, Intelligent Interface Board, 2-Line Display, RS-232 communication port, tare capability, and transducer connection terminals.

The Model 735 is powered continuously from its AC adapter or for up to 20 hours from our AA batteries. FREE Digiquartz® Interactive, Digiquartz® Assistant and Digiquartz® Terminal software are included to set up, configure, sample, plot and log data from the Model 735. [26]

**Characteristics**

Pressure gauge for external quartz resonant sensor.

8 units of pressure measurement + 1 programmable (hPa, kPa, bar, MPa, psi, mmHg, mH2O, inHg).

Resolution: $<$0.0001% FS (1 ppm, 6 digits).

Accuracy: +0.008% FS.

Alarms and configurable protection limits.

Functions of up and down speed, tare, temperature, etc.

Alphanumeric LCD display with 2 lines of 16 characters each line.

Robust quality desktop case.

Communication interface: RS-232.

Environmental conditions: from 0 °C to 40 °C

Power supply: Batteries (20 hours) or power supply from 6V to 25 V (DC).

Communication interface: RS232.

**It includes**

Manufacturer’s calibration certificate.

RS232 communication cable.

4 AA batteries and power supply for 220 V (AC).

Software (Windows) configuration and data logging.

## E.3.. Hti-Xintai digital Anemometer


Figure E.4: Hti-Xintai digital Anemometer [27]

**Characteristics**

11 selectable units of measure. Maximum range ± 2 psi

accuracy specification at: ± 0.3% FS

repeatability ± 0.2% (max.) ; ± 0.5 % FS

linearity / Hysteresis ± 0.29% FS

Dimensions are 5.79 ”x 2.16” x 1.26 ”in 4.58 oz, easy to use and transport.

Large LCD display with backlight and auto power off. The meter will automatically turn off after 20 minutes to extend battery life, easy to read the display in the dark.

One year warranty against manufacturing defects. Warranty is invalid if the meter has been opened.

# APPENDIX F. BELLMOUTH INLET DUCT BUDGET


**Precisgal Utillaje, S.L.U.**
Parque Tecnológico y Logístico de Vigo
Parcela 10.06, Calle B
36312 Beade, Vigo, Pontevedra (SPAIN)
TEL. +34 986 475 000
FAX. +34 986 475 001
www.precisgalgroup.com

**OFERTA Nº OFR190274** **Fecha:** 19/07/2019 **Cod.Prov.:**

**CLIENTE:** VASCO GALLEGA DE CALDERERÍA S.L.U.

**A la Attn.:** SR.PABLO ALVAREZ (telf. 673 019 111)/SR. ANTE M **Rev:1**

Muy Sres. Nuestros:
Nos complace enviarles presupuesto y plazo de entrega según su atenta consulta de referencia PET. OFERTA S/EMAIL A 14/07/2019 (telf. 673 019 111).
Confiando que será de su interés y en espera de sus noticias, aprovechamos la oportunidad para saludarles cordialmente.

| Pos. | Denominación | Referencia | Cantidad | Precio/ud (€) | Plazo |
|---|---|---|---|---|---|
| 5 | BELLMOUTH Ø66x79,77 -ALUMINIO 6061<br>Material: Aleación ALUMINIO 6061<br>Dimensiones:<br>longitud: 79.77 mm<br>diametro entrada: 66 mm<br>diametro salida: 50 mm<br>espesor: 2 mm<br>Eje semi mayor elipse: 49.77 mm<br>Eje semi menor elipse: 33.33 mm | PROTOTYPE | 1,00 | 360,00 | 7 SEMANAS |
| 15 | BELLMOUTH Ø66x79,77 -NYLON<br>Material: Nylon<br>Dimensiones:<br>longitud: 79.77 mm<br>diametro entrada: 66 mm<br>diametro salida: 50 mm<br>espesor: 2 mm<br>Eje semi mayor elipse: 49.77 mm<br>Eje semi menor elipse: 33.33 mm | PROTOTYPE | 1,00 | 250,00 | 7 SEMANAS |

**Total Oferta: 610,00 €**

**Notas:** Condiciones de envío: EX WORKS PRECISGAL

Forma de Pago: Cobro Contado

**Observaciones:**
REV.1 (16/10/2019) SE INCORPORAN POSICION ADICIONAL POR ALTERNATIVA DE MATERIAL FIBRA DE VIDRIO O PLASTICO, DE ACUERDO CON LO SOLICITADO POR EL CLIENTE.

Figure F.1: Bellmouth inlet duct budget